# Refined Estimates of Coseismic Subsidence along the Southern Cascadia Subduction Zone in Northern Humboldt Bay (Arcata Bay): Collaborative Research with University of Rhode Island and Humboldt State University

**External Grand Award Numbers: G14AP00128 and G14AP00129**

Investigators: Simon Engelhart[1], Eileen Hemphill-Haley[2], Harvey Kelsey[2], J. Scott Padgett[1]

1. Department of Geosciences, University of Rhode Island, 336 Woodward Hall, 9 East Alumni Avenue, Kingston, RI 02881, USA, engelhart@uri.edu

2. Geology, Humboldt State University, 1 Harpst Street, Arcata, CA 95521, USA, Eileen.Hemphill-Haley@humboldt.edu

Start date: September 1st 2014
End date: August 31st 2015

*Research supported by the U.S. Geological Survey (USGS), Department of the Interior, under USGS award numbers **G14AP00128 and G14AP00129**. The views and conclusions contained in this document are those of the authors and should not be interpreted as necessarily representing the official policies, either expressed or implied, of the U.S. Government.*

**Abstract**

We sampled three salt marshes along the northern margin of Humboldt Bay: Mad River Slough; McDaniel Slough; and Jacoby Creek. Field methods used gouge cores to map subsurface stratigraphic contacts. We collected core samples using Russian and 5cm diameter Fat Gouge hand driven coring devices at core locations that were representative of the overall stratigraphy at each study site. Analysis of the cores resulted in obtaining 23 new AMS radiocarbon dates, 86 samples documenting the fossil diatom assemblages, and 40 samples documenting the fossil foraminiferal assemblages. We collected 74 modern (surface) diatom samples to construct a local diatom transfer function. We sampled a subset of the modern samples for foraminifera to assess the applicability of a previously published foraminiferal transfer function from Oregon.

We find evidence for four coseismic subsidence events during the last 1700 years at Mad River Slough and McDaniel Slough, and three coseismic subsidence events during the same time period at Jacoby Creek. The youngest buried soil, soil A, has radiocarbon ages that are consistent with previous research throughout Cascadia, as well as within Humboldt Bay, that identify the youngest buried soil as the 250 yr BP (AD 1700) earthquake. We modeled the ages of three older coseismically buried soils using Oxcal. Revised age estimates for these coseismic subsidence events are: soil B, 924-816 cal yr BP; soil C, 1235-1018 cal yr BP; and soil D, 1634-1560 cal yr BP.

Transfer function analysis produced quantitative estimates of the amount of coseismic subsidence for the three buried soils (A, C, D) found at Jacoby Creek. Our new transfer function estimates of coseismic subsidence for the AD1700 provide a more precise constraint (0.1-0.9m) on a heterogeneous rupture model of this earthquake. Further, our diatom and foraminiferal analysis, coupled with chronology from AMS radiocarbon ages, demonstrate the potential for temporal variations in coseismic subsidence. In particular, there is evidence that the amount of coseismic subsidence was greater across soil contact D (at the 1634-1560 cal yr BP event) than for the earthquakes recorded by buried soils A and C. Further quantitative microfossil analysis of the buried soils at Mad River Slough and McDaniel Slough is required to substantiate these results.

## Context

Studies of coastal stratigraphy have helped to reconstruct the timing and magnitudes of past great earthquakes at the Cascadia subduction zone (e.g., Atwater, 1987; Nelson et al., 1996; Shennan et al., 1996; Atwater and Hemphill-Haley, 1997; Kelsey et al., 2002; Witter et al., 2003). Early research at Cascadia focused on identifying and mapping coastal stratigraphy consistent with megathrust rupture and radiocarbon dating bulk peat and plant fossils (e.g., Atwater, 1992; Nelson, 1992; Darienzo et al., 1994). Commonly, the stratigraphy of the AD 1700 earthquake was described, with the assumption that all earlier earthquakes were of a similar magnitude (M8.8-9.2). These early methods of estimating coseismic subsidence using lithology and plant macrofossils, foraminiferal, diatom, and pollen assemblages, had accompanying errors that were generally too large to distinguish differences between earthquake deformation from one earthquake to the next or between sites (e.g., Shennan et al., 1996; Atwater and Hemphill-Haley, 1997)

More recent research (e.g., Guilbault et al, 1996; Hawkes et al, 2011) has focused on reconstructing coseismic subsidence using microfossils in a fully quantitative method termed a transfer function. Transfer functions using foraminifera (e.g., Hawkes et al., 2011) or diatoms (e.g., Nelson et al., 2008) are capable of reconstructions with error terms ~±0.3m for typical Cascadia tidal ranges (2.0 to 2.8m), and the accuracy of these methods has been validated using a transplant experiment (Engelhart et al., 2013). The typical precision of these estimates allows for the understanding of how coseismic subsidence has varied both in time (different earthquakes at the same site) and in space (earthquakes of similar age at different sites). Understanding subduction zone earthquake variability over both space and time enables the development of more realistic models of the pattern of earthquake rupture.

Early models of earthquake rupture at Cascadia (e.g., Fluck et al., 1997; Wang et al., 2003; Leonard et al., 2004; 2010) were limited by the precision of the coseismic subsidence estimates. This restricted their ability to distinguish between patterns of subsidence produced by heterogeneous rupture. Initial Cascadia rupture models using uniform slip are inconsistent with modern instrumented megathrust ruptures produced by heterogeneous slip (e.g., Lee et al., 2011; Chlieh et al., 2007). Wang et al. (2013) used an improved dataset of high-precision transfer function estimates of coseismic land-level change that implies a more realistic heterogeneous model of rupture. However, while data coverage was good for Oregon and southern Washington, an absence of transfer function data south of latitude 43°N limited the ability of the model to fully resolve the rupture of the AD 1700 subduction zone earthquake. Previous paleoseismological investigations for Humboldt Bay provide valuable baseline data about the record of past Cascadia subduction zone earthquakes (e.g., Vick, 1988; Clarke and Carver, 1992; Jacoby et al., 1995; Pritchard, 2004; Valentine et al., 2012), but these data do not provide the refined estimates of coseismic subsidence required for a more realistic heterogeneous model of rupture (e.g. Wang et al., 2013). For instance, in a previous study, Pritchard (2004) was only able to constrain the subsidence for the AD 1700 earthquake to be 0 to 1.7 m. This project directly addresses the task of improving subsidence estimates both for the AD 1700 earthquake and earlier subduction zone earthquakes.

Anticipated project deliverables included:

1. Analysis of modern diatom samples and development of a local diatom transfer function from northern Humboldt Bay (i.e., Arcata Bay).

2. Collection of sediment cores from sites in northern Humboldt Bay to analyze for evidence of subduction zone earthquakes.

3. Analysis of AMS radiocarbon dates to produce a refined chronology for identified subduction zone earthquakes in northern Humboldt Bay.

4. Analysis of fossil diatom and foraminiferal samples.

5. Quantitative estimates of coseismic subsidence during prehistoric subduction zone earthquakes using diatom and foraminiferal transfer functions.

6. Presentation of results at scientific meetings.

7. Submission of results to peer-reviewed journals.

## 1. Summary of project deliverables

We sampled three sites along Arcata Bay, the northern lobe of Humboldt Bay: Mad River Slough, McDaniel Slough; and Jacoby Creek (Figure 1). We used gouge cores to understand the stratigraphy of each site before selecting cores that were representative of that stratigraphy. Representative copies of each buried soil were collected using either Russian or Fat Gouge hand driven coring devices. From core samples, we obtained 23 new AMS radiocarbon dates from all three sites. For calculating coseismic subsidence, we obtained 86 diatom and 40 foraminiferal samples from the Jacoby Creek site. We obtained 74 modern samples for developing a diatom transfer function and to assess the similarity of foraminiferal assemblages in Humboldt Bay to Oregon. We correlated buried soils among sites using the AMS radiocarbon results. We used a regional foraminiferal transfer function and a local diatom transfer function to estimate the amount of coseismic subsidence associated with three buried soils at Jacoby Creek. Initial results of our analyses have been presented at the 2015 Geological Society of America meeting in Baltimore and the 2015 American Geophysical Union Fall Meeting in San Francisco. We will commence submission of multiple papers for peer review by the end of 2016.

## 2. Study area

Arcata Bay is a depocenter for Holocene tidal and marsh sediment. Although situated on the deforming upper plate of the southern Cascadia subduction zone, Arcata Bay area is removed from the immediate effects of upper plate faults. The upper-plate Little Salmon fault is 12 km to the south, and the upper-plate Mad River fault zone is 10 km to the north (Kelsey and Carver, 1988; Clark and Carver, 1992) (Figure 1). There are no large rivers that discharge to the bay. Mad River Slough is a tidal inlet connected to Arcata Bay, but not permanently connected with

the Mad River, which flows directly to the ocean 5-6 km north of Arcata Bay. At infrequent, extremely high discharges, the Mad River overtops levees and partially spills into Arcata Bay via Mad River Slough. However, there is no sediment accumulation from the Mad River at the mouth of Mad River Slough, and such spillover is rare (for instance has occurred once - for less than a 24-hour period - in the last three decades) and has not affected sediment dispersal in Arcata Bay. There is no sedimentologic observations in either Mad River Slough cores, nor in the morphology of Arcata Bay at the outlet of Mad River Slough, from which one could infer prehistoric Mad River discharges that either built a delta into the bay or eroded tide marsh strata in lower Mad River Slough. Therefore, the margins of Arcata Bay respond to changes in relative sea level through tidal sedimentation during relative sea-level rise and emergence and coastal wetland soil development during relative sea-level fall.

Arcata Bay's north margin retreats north and progrades south in the course of the subduction zone earthquake cycle that affects the bay. For instance, immediately prior to the AD 1700 earthquake, Sitka spruce (*Picea sitchensis*) grew along at least part of the bay's north margin and these trees were killed by saline incursion following subsidence as a consequence of the AD 1700 earthquake (Jacoby et al, 1995). The marsh fringe bayward of the riparian tree zone similarly was inundated by tidal water after the AD 1700 subsidence (Vick, 1988; Pritchard, 2004). Such successive emergence and burial of marsh-fringing wetland soil environments will be documented in our lithostratigraphic, chronostratigraphic and biostratigraphic investigations.

## 3. Methods

### 3.1 Core Descriptions and Sampling

Grain size, sedimentary structures, contacts, thickness, and lateral and vertical facies changes were described in the field using general stratigraphic methods in combination with the Troels-Smith (1955) method for describing organic rich sediment. Cores were sampled using either the Russian or Fat Gouge depending on substrate type. Core samples were wrapped in plastic wrap and stored at 4 degrees Celsius. Sediment samples for diatom and foraminiferal analyses were collected from separate cores.

### 3.2 Surveying to sea-level datum

Sample elevations for each core and modern sample were obtained by using either direct RTK-GPS or through auto-leveling of each sample to a temporary benchmark, that was later measured using RTK-GPS. Data collected by the RTK-GPS was post-processed to obtain North American Vertical Datum 1988 (NAVD88) orthometric elevations. To establish elevations with respect to a tidal datum, we also took RTK-GPS measurements of the tidal benchmarks associated with a temporary tide gauge installation (12/01/1978 to 03/31/1979) at Mad River Slough (NOAA ID: 9418865). Modern sample elevations were converted to a Standardized Water Level Index (SWLI) to take into account tidal variations between sites (Engelhart et al., 2013).

## 3.3 Chronology

To identify the timing of coseismic subsidence, plant macrofossils were collected from the core material to provide 23 bracketing maximum and/or minimum ages for each event at all three sites (Table 1). We focused on samples that have the potential to tightly constrain the timing of coseismic subsidence, such as rhizomes of salt marsh plants that were living at the time of coseismic subsidence and that have a known relationship to the surface of the marsh (n=11), as well as detrital fragments of plants including stems and wood fragments (n=10), and seeds and seed casings (n=2). We combined the dates from all sites to develop Bayesian age models using Oxcal (Bronk Ramsey, 2009) and the IntCal13 calibration curve (Reimer et al., 2013) to estimate the timing of each coseismic subsidence event.

## 3.4 Diatoms

### 3.4.1 Sample Collection

To document the distributions of modern intertidal diatoms at northern Humboldt Bay, surface samples were collected along 3 leveled saltmarsh transects: Fay Slough transect 1 (FS1): Fay Slough transect 2 (FS2); and McDaniel Slough transect (MD) (Figure 1). At each locality, the transect extended from the supratidal levy surface – essentially an artificial upland – at the landward end of the marsh, across the entire salt marsh, and onto the adjacent unvegetated tidal flat. At the Fay Slough sites, transect samples from the unvegetated lower intertidal zone were collected over a range of elevations from the edge of the marsh to the bottom of the slough channel exposed at low tide. Transect samples from the tidal flat at McDaniel Slough were acquired from the soft mud surface over a distance of 25 m from the edge of the marsh. The vast tidal flat at this location extends for scores of meters with little change in elevation.

Modern diatom samples were collected at designated sites along each transect by scraping the upper few millimeters of surface sediment with a small metal spatula, and sealing the sample in a plastic bag. No preservatives were added, but the samples were immediately returned to the lab and refrigerated until ready to process.

Fossil (downcore) diatom samples were collected from Russian augur cores at intervals of 0.5 cm to 2 cm using a small metal spatula. These samples were similarly placed in labeled plastic bags and refrigerated until processed.

### 3.4.2 Lab Processing

For the diatom analyses, each microscope slide mount was prepared following a series of steps to ensure that both taxa distribution and concentration/abundance could be quantitatively compared among all samples. Both modern and downcore diatom samples were processed using the same procedure, as follows:

(1) A small (~1-2 cc) split of the sediment sample is placed in a 50 ml beaker and covered with 30% $H_2O_2$. Once the initial reaction ceases, additional $H_2O_2$ is added until it is evident that all organic material has been digested. The sample is then rinsed several times with distilled water, allowing the sample to rest undisturbed at least one hour between rinses.

The cleaned sediment residue is then transferred to a graduated centrifuge tube and diluted 10x in distilled water.

(2) Using a mechanical pipette, the dilute sample is thoroughly suspended by pumping the pipette a number of times, and then a 0.05 cc split of the diluted sample is extracted and evenly dispersed across a 22 mm × 30 mm glass coverslip that has been prewetted with distilled water. The coverslip is then left undisturbed to dry slowly at room temperature. Any coverslip that doesn't dry evenly is discarded and a new one prepared as equal distribution of particles on the coverslip is imperative for the analysis.

(3) Once dry, the coverslip is permanently affixed to a glass microscope slide with Naphrax® mounting medium.

Diatoms were counted using a Nikon 80i light microscope equipped with Nomarski interference contrast. Most were counted at a magnification of 650x, with all specimens tallied along 3 random vertical traverses, each traverse covering 8.8 $mm^2$ of the microscope slide (22 mm × the width of the field of view, which is 0.4 mm at 650x). The technique of counting all specimens over a certain area of the slide helps to document infrequent – but possibly paleoecologically significant – species that may be less likely to be encountered in the process of counting the first 300 taxa over a smaller proportion of the sample. For most samples, an average of about 400-600 diatoms were counted over 3 traverses, with a few particularly rich samples exceeding 1,000 valves, and each sample including one to a few species that were at least an order of magnitude more frequent than the majority of the taxa in the assemblage. A few samples contained very low diatom concentrations, in which case additional transects were completed to reach a minimum count of 300 valves.

In addition to the primary counts at 650x, an additional 5 random traverses were completed at low magnification (250x) on each slide to document occurrences of a group of unusually large taxa that may be underrepresented in counts completed at high magnifications. These are primarily lower intertidal epiphytic or epipelic diatoms with valves that measure several hundred micrometers in diameter for centric taxa (e.g., *Aulacodiscus* sp.), or along the longest (apical) axis for pennate species (e.g., larger *Gyrosigma* spp.). The occurrences, as well as preservation, of these larger taxa provide additional useful paleoecological information in the biostratigraphic analysis.

## 3.5 Foraminifera

Modern foraminiferal samples were collected at the same sites as the modern diatom samples (see section 2.4). Modern foraminiferal samples were immediately preserved in 30% ethanol buffered with calcium carbonate chips, and stained using rose Bengal. The rose Bengal permits the identification of foraminifera that were alive at the time of collection.

Both modern and fossil samples were analyzed by sieving through 500 and 63 micron sieves and retaining the sediment between those size fractions. The 500-micron sieve was checked for larger foraminifera before material was discarded. Additionally, modern

samples were split using a wet-splitter (Scott and Hermelin, 1993) after sieving to enable statistically significant counts to be obtained without the need to count the entire sample. Modern and fossil samples were analyzed until at least 200 dead foraminifera were identified, or until the entire sample was enumerated. Only samples with >40 foraminifera were used in the production of quantitative coseismic subsidence estimates.

## 3.6 Computerized Tomography and X-Ray

Contact sharpness and continuity is not always clear from optical inspection. Therefore, we followed recent studies in Cascadia (e.g., Milker et al., in press) and Alaska (e.g., Briggs et al., 2014) and obtained high-resolution imagery in order to analyze fossil core density contrasts. Computerized tomography scans were conducted at Oregon State University College of Veterinary Medicine, following the methods outlined in Rothwell and Rack (2006) and Davies et al. (2011). Density measurements were performed using a Toshiba Aquilion 64 Slice. Scans were collected at 120 kVp and 200 mA and a pitch of 0.5s (100 mAs). For visualization purposes, the resulting images were processed with a "bone" algorithm to generate coronal images every mm across the core. X-ray diffraction scans were taken at the University of Rhode Island Health Services, Radiology Lab on a FujiFilm, FCR XL-2, high-quality digital X-ray machine with a human lower leg density setting at 16 KV and 4.5 mAs.

# 4. Results

## 4.1 Stratigraphy

### 4.1.1 Jacoby Creek

The stratigraphy of the southern section of Jacoby Creek marsh has previously been analyzed (Pritchard, 2004). We extended this analysis to the marsh region to the north bordering G Street (Figure 1). Our new analysis identifies three buried soils that are likely representative of three coseismic subsidence events during the past 1700 years (Figure 2a). This represents one additional soil compared to the two identified by Pritchard (2004).

### 4.1.2 McDaniel Slough

The stratigraphy beneath distal salt marshes at McDaniel Slough has previously been analyzed (e.g., Pritchard, 2004). We focused our investigation on the western-most of the sites previously investigated by Pritchard (Figure 1). Our new analysis presented here identifies four buried soils that are likely representative of four coseismic subsidence events during the past 1700 years (Figure 2b). This represents two additional soils compared to the two identified by Pritchard (2004).

### 4.1.3 Mad River Slough

The stratigraphy of the lower Mad River Slough has previously been analyzed (e.g., Vick, 1988; Valentine et al., 2012). We reoccupied the coring sites of Vick (1988) in the lower Mad River Slough where samples were most likely to reflect intertidal deposition both above and below buried soils (Figure 1). Our new analysis presented here identifies four buried soils that are likely representative of four coseismic subsidence event during the past 1700 years (Figure 2c). This is consistent with the four "well-defined cycles of peat overlain by mud" described by Vick (1988).

## 4.2 Chronological data

We obtained 23 new AMS radiocarbon dates (Table 1) to refine our understanding of the timing of coseismic subsidence in Arcata Bay. These ages consisted of both maximum and minimum constraints. We utilized the dates to construct an age model using Oxcal and the phase approach (Bronk Ramsey, 2009). We determine that contact A was deposited by the 250 yr BP (AD 1700) earthquake in line with previous research in Arcata Bay and consistent with young maximum radiocarbon ages in the soil (three dates ranging from 170-235 $^{14}$C years). We do not model the age of the youngest buried soil due to the limitations of radiocarbon imposed by a plateau in the calibration curve post AD 1650. The assumption that this soil represent the AD 1700 earthquake is consistent with the tsunami modeling of Satake et al. (2003). The modeled ages for the three earlier earthquakes are 924-816 cal yr BP (contact B), 1235-1018 cal yr BP (contact C), and 1634-1560 cal yr BP (contact D).

## 4.3 Microfossil Analysis

### 4.3.1 Modern Diatom Analysis

This study represents the first detailed census of diatoms from intertidal environments of Humboldt Bay. Surface samples were collected for diatoms along horizontal transects at three localities (Figure 1, Figure 3): a marsh and tidal flat on the northeastern shore of Humboldt Bay ("McDaniel Slough transect"); and 2 transects along Fay Slough ("FS1" and "FS2"). Fay Slough is inland arm of the larger Freshwater Slough which connects to the south shore of Arcata Bay. We additionally collected a few bottom samples by boat from muddy shoals in the northwestern part of the bay south of the mouth of Mad River Slough.

McDaniel Slough marsh and Fay Slough were chosen for collecting modern diatom samples for two principle reasons. First, compared to most of the shores and sloughs along Humboldt Bay, these locations have relatively intact salt marshes. Intact salt marshes represent a minor fraction of the vast salt marshes that once extended inland from the bay the past (Laird, 2013). The McDaniel Slough marsh has also been impacted by *Spartina densiflora* (dense-flowered cordgrass), an invasive plant species native to Chile that was probably introduced into Humboldt Bay in the late 1800s (Pickart, 2001). Dense overgrowths of *Spartina* can suppress productivity of microalgae, including diatoms, because of diminished light penetration to the marsh surface (Augyte and Pickart, 2011). Although *S. densiflora* is dispersed across the marsh at the McDaniel Slough transect location, it has not displaced the natural groundcover, *Spartina virginica* (pickleweed). Diatoms are equally or more abundant at McDaniel Slough than at Fay Slough where *Spartina* was not observed (Figure 4).

The second reason we chose the McDaniel Slough and Fay Slough transect locations was because they are currently accumulating deposits comparable to what we observed in the subsurface: fine-grained clastic deposits consistent with mudflats, and muddy to densely rooted peaty deposits consistent with organic-rich (O-horizon) soils formed in low and high marshes as well as in drier soils at the transition from marsh to upland. Other marsh and tidal flat localities along Humboldt Bay with dominantly sandy substrate would have provided poor modern analogues for the downcore material.

The initial modern dataset included a total of 74 samples from the three transect locations and the shoals off Mad River slough. Of these, 13 were recovered from active channels and showed evidence for mixed and winnowed diatom assemblages, and therefore were excluded from the training set. The remaining 61 modern samples provide a fair balance of representative samples for different intertidal to supratidal environments at the sampling sites (Figure 5). From these 61 transect samples, a modern training set of about 140 species and varieties of benthic diatoms was compiled for use in the transfer function analysis (Table 2). Allochthonous planktonic taxa observed in the modern assemblages were recorded but are not included in the training set.

Comparisons of the modern and downcore assemblages showed strong similarities in species composition. For example, of the 80 most common diatom taxa observed in the modern samples, i.e., taxa that totaled > 2% of at least one sample, 62 (78%) were also observed in downcore samples from Jacoby Creek marsh. Conversely, of the 78 most abundant diatom species observed in our core samples from Jacoby Creek marsh, 62 species (80%) were also observed in one or more surface samples. The relative abundances of some taxa vary greatly in the surface samples as compared to their occurrences in the core samples. This variability in species abundances between surface and fossil deposits is a standard occurrence in diatom studies, an artifact of taphonomy (i.e., preservation potential) and possibly past variability in species dominance at a site. This variability, though common and predictable, is problematic in that it can negatively affect the outcome of modern-analogue evaluations using diatom samples, making such analogues either difficult (Kemp and others, 2009; Watcham and others, 2013) or impossible (Wilson and Lamb, 2012) to establish. For this study, the comparable occurrences of many species in both the surface and downcore samples shows that the kind of brackish-marine intertidal environment that we sampled along the transects likely persisted in northern Humboldt Bay for most of the duration of most of our 1,700-year core record.

Notable taxa that were prominent in surface samples but to date have not been observed in the stratigraphic record at Humboldt Bay are the marsh species *Diploneis ovalis* and *D. didyma*. These are cosmopolitan salt marsh taxa (Vos and de Wolf, 1993a,b; Witkowski and others, 2000) with sturdy, relatively dissolution-resistant valves. Their absence in the downcore deposits, therefore, is not a result of poor preservation. At both McDaniel Slough and Fay Slough these taxa co-occur with *D. interrupta*, a marsh species with a similar dissolution-resistant valve structure that is also prominent in a number of subsurface samples. It is possible that these varieties of *Diploneis* may be found at other coring locations along Humboldt Bay as additional work continues. Other taxa that were excluded from the transfer function analysis include the tychoplanktonic species *Paralia sulcata*, and the benthic species *Tryblionella granulata.* The modern-diatom sample counts showed that these taxa were both abundant and widely dispersed across the intertidal transects and not strongly diagnostic of a particular intertidal elevation (Figure 6). Further, the fossil counts showed that, because of their heavily silicified, dissolution-resistant valves, these taxa were anomalously concentrated in many downcore samples. Anomalous concentrations of dissolution-resistant taxa such as *P. sulcata*

and *T. granulata* are a common occurrence in coastal biostratigraphic studies using diatoms (for example, Atwater and Hemphill-Haley, 1997, their figure 17).

### 4.3.2 Modern Foraminiferal Analysis

A subset of the modern dataset from Faye Slough transect 1 was analyzed to compare the results to those obtained from multiple marsh transects used in the regional Oregon foraminiferal transfer function (e.g., Engelhart et al., 2013; Milker et al., in press). Samples within the high and middle salt marsh are dominated by the same foraminifera as Oregon, including *Balticammina pseudomacrescens*, *Trochammina inflata*, *Haplophragmoides spp.*, and *Jadammina macrescens*. Further, in line with the results from Oregon, the low marsh and tidal flat species *Miliammina fusca* increases in abundance with depth, with a dominance below MHW. These observations suggest that the Oregon foraminiferal transfer function is broadly representative of the assemblages found in Arcata Bay.

### 4.3.3 Microfossil Analyses

Soil Contact D (1634-1560 cal yr BP)

We analyzed microfossils across contact D between 168.5-177 cm depth in core JC1402A. The lower part of buried soil D, between 172-176 cm, is faint and includes variable organic content implied from color changes from brown-gray to pale gray (Figure D6-B). The upper part of the buried soil is more distinct, consisting of dark brown to black muddy peat. The soil D contains ~ 0.5-1.0 cm diameter wood or root fragments at 170 and 177 cm. The top of the soil forms a distinct contact with overlying clastic sediment consisting of gray-brown (162-168 cm) to gray (150-162 cm) mud. Organic fragments up to 1 cm diameter were observed immediately above the soil at 167 cm, as well as in gray mud at 159 cm and 161 cm. Minor variations in the depths of stratigraphic units are noted between the diatom and foraminifera cores.

The diatom data show that soil D at this site accumulated on a dry upland surface and not a salt marsh. Gray, massive silty mud underlyng the soil is devoid of diatoms with the exception of a few fragments of freshwater taxa in some samples (Figure 7). In contrast, diatoms are common in the muddy deposits above the soil, with assemblages dominated by lower intertidal species (e.g., *Caloneis westi*, *Trachyneis aspera*, *Surirella fasciculata*, *Navicula digitoradiata, Gyrosigma* spp.), consistent with a tidal flat. Freshwater and terrestrial diatoms including *Hantzschia amphioxys* (species #1 on Figure 8), *Stauroneis* spp., and *Eunotia* spp. are present in the soil, as well with a few phytoliths in samples at 169 cm and 176 cm. Very rare occurrences of the mudflat taxa in the upper part of the soil (Figure 7) are not in place but rather an artifact of the overlying mud being mixed into the interstices of the upland soil after burial. The diatom assemblages in the first cm of mud above the soil are not well preserved, but good preservation in the remaining samples in the overlying mud suggests accumulation on a tidal flat without intense reworking.

The foraminiferal data also show evidence of mixing in the soil to a depth of 6cm below the contact (170cm; Figure 9). Low abundance assemblages 6cm below the contact suggest the incorporation of foraminifera down into the soil (e.g., Engelhart et al., 2013; Milker et al., in press). While foraminiferal abundances in the top 2cm of the soil are consistent with other soils

at Jacoby Creek (>200 individuals), the decreasing abundance of foraminifera with distance below the contact is consistent with mixing (e.g., Milker et al., 2015), supported by the dry upland interpretation from the diatom assemblage. The assemblage in these two samples is composed of *T. inflata* (38-47%), *J. macrescens* (25-38%), *B. pseudomacrescens* (9-10%), and *M. fusca* (12-15%). Samples above the buried soil have high abundances and appear to be in-situ assemblages. The assemblage in the two cm above the soil is dominated by *Trochammina inflata* (46-52%) and *Jadammina macrescens* (31-38%), with the presence of *Miliammina fusca* (11-18%) and is consistent with a marsh environment forming close to but below MHW.

The amount of subsidence accompanying the contact D earthquake (1634-1560 cal yr BP) at this site is estimated at > 1.5 m based on the fossil diatom data (Figure 7) and > 0.5m based on the fossil foraminiferal data (Figure 9). Note that there is a discrepancy between the fossil diatom and foraminiferal assemblages, especially for the samples in the mud above contact D: the complete absence of salt marsh diatom taxa is inconsistent with fossil saltmarsh foraminifera. However, because fossil diatom assemblages indicate a shift from upland to tidal flat, we infer a major change in environment at this site coincident with the earthquake. Further analyses, both within this core and at the other sites, will attempt to reconcile this discrepancy.

There is a disagreement between the foraminiferal and diatom elevation estimates for the samples in the mud above contact D. This discrepancy will be investigated both within this core, and at the other sites. However, as the estimate is a minimum, the subsidence estimates are not in disagreement.

Soil Contact C (1235-1018 cal yr BP)

The contact C soil in core JC1402A at Jacoby Creek consists of peaty mud between 126.5-132 cm depth. The soil is better developed and less muddy, and has darker coloration (dark brown with black layers) above 130 cm (Figure 10-B). Both the upper and lower contacts of the soil are slanted at shallow angles relative to the core barrel, possibly a disruption during coring. The top of the soil is clearly discernible relative to overlying gray mud, but the peaty mud of the soil is so fine grained that there is no distinctive textural change from one unit to the other. The depth of contact C varies over 6cm between the diatom and foraminifera cores.

Soil C is underlain by decimeters of gray mud, slightly more organic-rich in the interval below 154 cm to the base of the core at 160 cm. Above the soil, a 3-3.5 cm cap of massive gray mud grades upwards to brownish gray mud with common organic fragments that extends from 121 cm to the top of the core at 110 cm.

The lower part of the soil between 129-131 cm contains an assemblage dominated by *Diploneis interrupta* and *Nitzschia sigma* (species #12 and 20 in Figure 8), consistent with a salt marsh environment regularly flooded by tides. This assemblage is replaced in the upper soil by a mix of well-preserved species indicative of higher, drier marshes found near and above MHHW, including *Pinnularia lagerstedtii*, *Luticola mutica*, *Cosmioneis pusilla*, *Frustulia linkeii*, *Tryblionella debilis*, and *Caloneis bacillum* (species #2, 3, 5, 6, 10, and 11 on Figure 8).

Therefore, the soil development at this site shows a transition over time from a salt marsh regularly flooded by tides to a more aerophile, infrequently inundated marsh environment. In contrast, diatoms in the overlying clastic deposits are consistent with a muddy lower intertidal environment at the transition from tidal flat to low marsh, an observation supported both by the kinds of diatoms present as well as the amount of plant fragments visible in the mud. Prominent diatoms in the muddy deposits in the upper part of the core include *Gyrosigma wansbeckii*, *G. balticum*, *Tryblionella apiculata*, *Caloneis westii*, *Trachyneis aspera*, *Nitzschia fasciculata*, and *Surirella fastuosa* (species #29, 30, 33, 36, 38, 42, and 48 on Figure 8).

Foraminifera in gray mud beneath the contact C soil (160-144cm; Figure 11) dominantly consist of *J. macrescens* (43-64%) and *T. inflata* (23-32%), with less frequent *B. pseudomacrescens* (1-19%) and *M. fusca* (1-13%). This is consistent with a middle marsh occurring between MHW and MHHW. Three samples between 132-135 cm depth in the soil directly below the contact are associated with an increase in *B. pseudomacrescens* (48-69%), and associated decreases in *J. macrescens*, *T. inflata*, and *M. fusca*, suggesting a high marsh forming at or above MHHW. Samples in the mud above the soil return to dominance by *J. macrescens* (62-71%), with increased *M. fusca* (3-27%) and a decrease in *B. pseudomacrescens* (0-3%). This is indicative of a middle to low marsh transition around MHW.

Coseismic subsidence (i.e., abrupt RSL rise) accompanying the contact C earthquake (1235-1018 cal yr BP) at this locality is estimated at 0.7 ± 0.29 m, based on a distinct shift in fossil diatom assemblages between the top of the soil (126.5 cm) to the lowest sample in the overlying mud that is interpreted as in place (121 cm). The first few centimeters of mud capping the soil contains a mixture of poorly preserved taxa consistent with a reworked deposit, and therefore assemblages in this interval are not used for the RSL reconstruction. Also, the reconstruction is based on a calibration excluding the lower intertidal species *Diploneis bombus*. *D. bombus* is a cosmopolitan tidal flat species, abundant in lower intertidal samples from Humboldt Bay, with presumably allochthonous valves found only in low numbers in a few marsh samples (Figure 12-A). Its relatively high abundance (> 5%) in some of the soil samples (Figure 12-B) is interpreted as an artifact of taphonomy, with unusual concentrations of its dissolution-resistant valve retained in the clastic sediment on which the marsh developed. Diverse and well-preserved high-marsh/aerophilous taxa are consistent with the soil being positioned near or above MHHW, with SWLI values of > 100 expected for the reconstruction (Figure 10). Because the preferred elevation (optimum) for *D. bombus* derived by the model falls in the lower intertidal zone (Figure 8, species # 56), its presence in the soil samples effectively suppresses the reconstructed elevation of the soil, with results for the upper part of the soil (<100 SWLI) that are inconsistent with the dominant occurrences of well-preserved marsh taxa that are very likely in place. The absence of *D. bombus* from the non-soil (muddy) samples in the core does not strongly impact the reconstructed elevations for those samples because of the common occurrences of other tidal flat taxa to fuel the reconstruction.

The foraminiferal-based transfer function estimates coseismic subsidence accompanying the contact C earthquake at 0.37 ± 0.24 m (Figure 11) based on the sample at the top of the soil,

and a sample equivalent to the first diatom sample that showed an in place assemblage not influenced by reworking (5.5cm above the soil).

Absence of Contact B at Jacoby Creek

Jacoby Creek differs from Mad River Slough and McDaniel Slough in the absence of contact B. After obtaining CT scans of our cores, we identified a change in density below the 250 yr BP earthquake horizon that may represent contact B (Figure 14, at 100 cm). However, two radiocarbon ages obtained from below this contact (Table 1) are stratigraphically inconsistent, possibly indicating the re-deposition of older material. Coupled to evidence from diatoms around this contact (97 and 99 cm) that indicate a winnowed or eroded deposit, we hypothesize that contact B may have been eroded at Jacoby Creek sometime prior to the 250 yr BP earthquake.

Soil Contact A (250 yr BP)

The 250 yr BP buried soil (contact A) is between 77-92 cm depth in core JC11402A (Figure 13), ranging from a faint brown organic mud in the lower part of the soil (85-92 cm) to brown muddy fibrous peat in the upper part (77-85 cm). The upper contact of the soil with overlying gray mud is not sharp and horizontal, but rather the uppermost 1-2 cm of the soil is disrupted and irregular, with mud infilling spaces between peaty material. Underlying the soil, to the base of the core at 110 cm, is gray to brownish-gray mud with minor amounts of plant fragments, and including a brown organic-rich layer near 106 cm. Gray mud caps the soil, extending to the top of core at 60 cm. The lowermost 2-3 cm of the mud, between ~ 74-76 cm depth, is massive but above 76 cm it is faintly and irregularly laminated. A 1cm variation in the depths of stratigraphic units are noted between the diatom and foraminifera cores.

Diatom assemblages dominated by *Diploneis interrupta* in the upper part of the 250 cal yr BP soil suggest a high salt marsh frequently inundated by tides. This assemblage is comparable to the assemblage in the lower part of soil C (1235-1018 cal yr BP), and different from the upper part of soil C where dominant high-marsh/aerophilous diatoms indicate higher and drier elevations near or above MHHW. The mud overlying the 250 yr BP soil includes a diverse array of lower intertidal taxa, including *Nitzschia scapelliformis*, *Gyrosigma wansbeckii, G. balticum*, *Caloneis westii*, *Scolioneis tumida*, *Tryblionella apiculata*, *T. acuminata*, and *Diploneis bombus* (Figure 8, species #24, 29, 30, 33, 43, 48, and 56).

Foraminifera in the 250 yr BP soil (Figure 14) dominantly consist of *B. pseudomacrescens* (20-58%), *T. inflata* (24-42%), and *J. macrescens* (17-41%). This is consistent with a soil forming near MHHW. Samples in the gray mud overlying the soil show an increasing abundance upcore of *M. fusca* (3 to 17%) and *J. macrescens* (38 to 56%), associated with a decreasing abundance upcore of *B. pseudomacrescens* (24 to 2%) and *T. inflata* (31 to 16%).

The diatom-based transfer function reconstruction shows 0.59 ± 0.28 m of subsidence coincident with the 250 yr BP earthquake (Figure 12), based on a shift in diatom assemblages from the upper part of the soil at 77 cm, which is interpreted as in place and not mixed with mud across the disrupted soil-mud contact, and the mud sample at 73 cm, which is the lowest

muddy sample that contains a well preserved assemblage and does not show evidence for strong reworking. Diatoms in muddy samples underlying the soil are consistent with lower intertidal deposits, with some samples containing few diatoms relative to background sedimentary particles compared to other samples in the core. Low-diversity, poorly preserved assemblages at 97 cm and 99 cm suggest an eroded or winnowed deposit in that interval.

The foraminiferal-based transfer function reconstruction shows 0.30 ± 0.24 m of subsidence (Figure 14) associated with the 250 yr BP earthquake (Figure 13), based on the top sample in the soil and the first foraminiferal sample above the soil not associated with the region of strong reworking identified by the diatom analysis.

Taking the ranges of the diatom and foraminiferal transfer function estimates, we conservatively estimate subsidence during the 250 yr BP earthquake of 0.1-0.9m. Further refinement of this estimate will be achieved by analysis of the samples from multiple sites at Mad River Slough and McDaniel Slough, and the further development of the transfer functions to include more samples outside of the local region (diatoms) and to incorporate a Humboldt Bay transect (foraminifera). Our new estimate is a considerable improvement on the estimate of Pritchard et al. (2004) of 0-1.7m.

## 5. Conclusions

1. On the north margin of Humboldt Bay at the three Arcata Bay paleoseismic sites, we find evidence for four coseismic subsidence events at two marshes (Mad River Slough and McDaniel Slough) and three subsidence events at one marsh (Jacoby Creek). We hypothesize that the absence of contact B at Jacoby Creek is due to erosion.

2. Evidence for sudden and lasting coseismic subsidence is supported by quantitative diatom and foraminiferal data at the Jacoby Creek site, and by stratigraphic features including sharp upper contacts between peat and mud at all locations.

3. Based on radiocarbon ages and previous research, we identify contact A as the 250 BP (AD1700) earthquake. The modeled ages of the three older coseismic subsidence events based on a suite of maximum and minimum ages are 924-816 cal yr BP, 1235-1018 cal yr BP, and 1634-1560 cal yr BP.

4. Our quantitative analysis has reduced the uncertainty associated with the subsidence caused by the 250 BP (AD1700) earthquake from 0-1.64m (Pritchard, 2004) to 0.1-0.9 m. Refinement of this estimate will be possible with additional quantitative diatom and foraminiferal analyses at the Mad River Slough and McDaniel Slough sites and from further improvement of the transfer functions.

5. Diatom and foraminiferal evidence suggest that similar subsidence was observed for the 250 yr BP (0.1-0.9m) and 1235-1018 cal yr BP (0.1-1.0m) earthquakes. In contrast, based on the diatom evidence the 1634-1560 cal yr BP earthquake likely produced greater than 1.5m of

subsidence. The above results suggest that there have been temporal variations in subsidence at Arcata Bay during the past 1700 years. Quantitative microfossil analyses of the 924-816 cal yr BP earthquake at Mad River Slough and McDaniel slough will further elucidate variations in coseismic subsidence during the past 1700 years.

## References Cited


Atwater, B.F., 1987. Evidence for great Holocene earthquakes along the outer coast of Washington state. Science 236, 942-944.

Atwater, B.F., 1992. Geologic evidence fo earthquakes during the past 2000 years along the Copalis River, southern coastal Washington. Journal of Geophysical Research Solid Earth, doi:10.1029/91JB02346.

Atwater, B.F., Hemphill-Haley, E., 1997. Recurrence intervals for great earthquakes of the past 3500 years at northeastern Willapa Bay, Washington. U.S. Geological Survey Professional Paper 1576, 108 pp.

Augytė, S., Pickart, A., 2011. Algal response to removal of the invasive cordgrass Spartina densiflora in a salt marsh at Humboldt Bay, CA. Unpublished report, U.S. Fish and Wildlife Service, Humboldt Bay National Wildlife Refuge, 13 p.

Briggs, R.W., Engelhart, S.E., Nelson, A.R., Dura, T., Kemp, A.C., Haeussler, P.J., Corbett, D.R., Angster, S.J., Bradley, L-A., 2014. Uplift and subsidence reveal a nonpersistent megathrust rupture boundary (Sitkinak Island, Alaska). Geophysical Research Letters, 10.1002/2014GL059380.

Bronk Ramsey, C. 2009. Bayesian analysis of radiocarbon dates. Radiocarbon 51(1), 337-360.

Chlieh, M., Avouac, J.-P., Hjorleifsdottir, T.-R., Song, A., Ji, C., Sieh, K., Sladen, A., Hebert, H., Natawidjaja, D.H., Galetzka, J., 2007. Coseismic slip and afterslip of the great $M_w$9.15) Sumatra-Andaman earthquake of 2004. Bulletin of the Seismological Society of America 97, S152-S173.

Clarke, S. H., Carver, G. A., 1992, Late Holocene Tectonics and Paleoseismicity, Southern Cascadia Subduction Zone, Science, 255, 188-192.

Darienzo, M.E., Peterson, C.D., and Clough, C., 1994, Stratigraphic evidence for great subduction-zone earthquakes at four estuaries in northern Oregon, U.S.A. Journal of Coastal Research, v. 10, p. 850-876.

Davies, M.H., Mix, A.C., Stoner, J.S., Addison, J.A., Jaeger, J., Finney, B., Wiest, J., 2011. The deglacial transition on the southeastern Alaska Margin: meltwater input, sea level rise, marine productivity, and sedimentary anoxia. Paleoceanography 26, doi:10.1029/2010PA002051.

Engelhart, S.E., Horton, B.P., Nelson, A.R., Hawkes, A.D., Witter, R.C., Wang, K, Wang, P-L., Vane, C.H., 2013. Testing the use of microfossils to reconstruct great earthquakes at Cascadia. Geology 41, 1067-1070.

Fluck, P., Hyndman, R.D., Wang, K., 2007. Three-dimensional dislocation models for great earthquakes of the Cascadia subduction zone. Journal of Geophysical Research 102, 539-550.

Guilbault, J.P., Clague J.J., Lapointe, M., 1996. Foraminifera evidence for the amount of coseismic subsidence during a late Holocene earthquake on Vancouver Island, west coast of Canada. Quaternary Science Reviews 15, 913-937.

Hawkes, A.D., Horton, B.P., Nelson, A.R., Vane, C.H., Sawai, Y., 2011. Coastal subsidence in Oregon, USA, during the giant Cascadia earthquake of AD 1700. Quaternary Science Reviews 30, 364-376.

Jacoby, G., Carver, G. and Wagner, W., 1995, Trees and herbs killed by an earthquake ~300 yr ago at Humboldt Bay, California. Geology 23,77-80.

Kelsey, H.M., and Carver, G.A., 1988, Late Neogene and Quaternary tectonics associated with the northward growth of the San Andreas transform fault, northern California. Journal of Geophysical Research 93, 4797-4819.

Kelsey, H.M., Witter, R.C., Hemphill-Haley, E., 2002. Plate-boundary earthquakes and tsunamis of the past 5500 yr, Sixes River estuary, southern Oregon. Geological Society of America Bulletin 114, 298-314.

Laird, A., 2013. Humboldt Bay shoreline inventory, mapping and sea level rise vulnerability assessment. Unpublished report prepared for State Coastal Conservancy, Oakland, California, 158 pp.

Lee, S.-J., Buang B.-S., Ando, M., Chiu, H.-C., Wang, J.-H., 2011. Evidence of large scale repeating slip during the 2011 Tohoku-Oki earthquake. Geophysical Research Letters, 38, L19306.

Leonard, L.J., Hyndman, R.D., Mazzotti, S., 2004. Coseismic subsidence in the 1700 great Cascadia earthquake: Coastal estimates versus elastic dislocation models. Geological Society of America Bulletin 116, 655-670.

Leonard, L.J., Currie, C.A., Mazzotti, S., Hyndman, R.D., 2010. Rupture area and displacement of past Cascadia great earthquakes from coastal coseismic subsidence. Geological Society of America Bulletin 122, 2079-2096.

Milker, Y., Horton, B.P., Nelson, A.R., Engelhart, S.E., Witter, R.C., 2015. Variability of intertidal foraminiferal assemblages in a salt marsh, Oregon, USA. Marine Micropaleontology 118, 1-16.

Milker, Y., Nelson, A.R., Horton, B.P., Engelhart, S.E., Bradley, L-A., Witter, R.C., in press. Differences in coastal subsidence in southern Oregon (USA) during at least six prehistoric megathrust earthquakes. Quaternary Science Reviews, doi:10.1016/jquascirev.2016.04.017

Nelson, A.R., 1992. Holocene tidal-marsh stratigraphy in south-central Oregon – Evidence for localized sudden submergence in the Cascadia subduction zone. In: Fletcher, C.P., Wehmiller, J.F. (eds.), Quaternary coasts of the United States – Marine and Lacustrine systems, Oklahoma. Society for Sedimentary Geology Special Publication No. 48, 287-301.

Nelson, A.R., Jennings, A.E., and Kashima, K., 1996. An earthquake history derived from stratigraphic and microfossil evidence of relative sea-level change at Coos Bay, southern coastal Oregon. Geological Society of America Bulletin 108, 141–154.

Nelson, A.R., Sawai, Y., Jennings, A.E., Bradley, L-A., Gerson, L., Sherrod, B., Sabean, J., Horton, B.P., 2008. Great-earthquake paleogeodesy and tsunamis of the past 2000 years at Alsea Bay, central Oregon coast, USA. Quaternary Science Reviews 27, 747-768.

Pickart, A., 2001. The distribution of Spartina densiflora and two rare salt marsh plants in Humboldt Bay 1998-1999. Unpublished report, U.S. Fish and Wildlife Service, Humboldt Bay National Wildlife Refuge, 25 pp.

Pritchard, C. J., 2004. Late Holocene relative sea level changes, Arcata Bay, California: Evaluation of Freshwater Syncline movement using coseismically buried soil horizons, [M.S.Thesis]. Humboldt State University, Arcata, California, 56 pp.

Reimer, P.J., Bard, E., Bayliss, A., Beck, J.W., Blackwell, P.G., Bronk Ramsey, C., Buck, C.E., Cheng, H., Edwards, R.L., Friedrich, M., Grootes, P.M., Guilderson, T.P., Haflidason, H., Hajdas, I., Hatte, C., Heaton, T.J., Hoffmann, D.L., Hogg, A.G., Hughen, K.A., Kaiser, K.F., Kromer, B., Manning, S.W., Niu, M., Reimer, R.W., Richards, D.A., Scott, E.M., Southon, J.R., Staff, R.A., Turney, C.S.M., van der Plicht, J., 2013. IntCal13 and Marine13 radiocarbon age calibration curves 0-50,000 years cal BP. Radiocarbon 55(4), 1869-1887.

Rothwell, R.G., Rack, F.R., 2006. New techniques in sediment core analysis: an introduction. Geological Society, London 1-29, doi:10.1144/GSL.SP.2006.267.01.01

Satake, K, Wang, K., Atwater, B.F., 2003. Fault slip and seismic moment of the 1700 Cascadia earthquake inferred from Japanese tsunami descriptions. Journal of Geophysical Research 108, doi:10.1029/2003JB002521.

Scott, D.B., Hermelin, J.O.R., 1993. A device for precision splitting of micropaleontological samples in liquid suspension. Journal of Paleontology 67, 151-154.

Shennan, I., Long, A.J., Rutherford, M.M., Green, F.M., Innes, J.B., Lloyd, J.M., Zong, Y., Walker. K.J., 1996. Tidal marsh stratigraphy, sea-level change and large earthquakes, i: a 5000 year record in Washington, USA. Quaternary Science Reviews, 1023-1059.

Troels-Smith, J., 1955. Karakterisering af lose jordater Danmarks Geologiske Undersogelse Series IV. 3 (10), 73pp.

Valentine, D.W., Keller, E.A., Carver, G., Li, W.-H., Manhart, C., Simms, A.R., 2012. Paleoseismicity of the southern end of the Cascadia subduction zone, northwestern California. Bulletin of the Seismological Society of America 102, 1059-1078.

Vick, G.S. 1988, Late Holocene paleoseismicity and relative sea level changes of the Mad River Slough, Arcata Bay, California, [M.S.Thesis]: Arcata, California, Humboldt State University, 87 pp.

Vos, P.C., de Wolf, H., 1993a. Diatoms as a tool for reconstructing sedimentary environments in coastal wetlands; methodological aspects. Hydrobiologia 269/270, 285–296.

Vos, P.C., de Wolf, H., 1993b. Reconstruction of sedimentary environments in Holocene coastal deposits of the southwest Netherlands; the Poortvliet boring, a case study of palaeoenvironmental diatom research. Hydrobiologia 269(1), 297–306.

Wang, K., Wells, R., Mazzotti, S., Hyndman, R.D., Sagiya, T., 2003. A revised dislocation model of interseismic deformation of the Cascadia subduction zone. Journal of Geophysical Research 108, 2026.

Wang, P.-L., Engelhart, S.E., Wang, K., Hawkes, A.D., Horton, B.P., Nelson, A.R., Witter, R.C., 2013. Heterogeneous rupture in the great Cascadia earthquake of 1700 inferred from coastal subsidence estimates. Journal of Geophysical Research 118, 1-14.

Watcham, E., Shennan, I., Barlow, N., 2013. Scale considerations in using diatoms as indicators of sea level change: lessons from Alaska. Journal of Quaternary Science 28, 165-179.

Wilson, G.P., and Lamb, A.L., 2012, An assessment of the utility of regional diatom-based tidal-level transfer functions: Journal of Quaternary Science 27(4), 360–370.

Witkowski, A., Lange-Bertalot, H., and Metzeltin, D., 2000. Diatom flora of marine coasts: Iconographica Diatomologica 1, 925 p.

Witter, R.C., Kelsey, H.M., Hemphill-Haley, E., 2003. Great Cascadia earthquakes and tsunamis of the past 6700 years, Coquille River estuary, southern coastal Oregon. Geological Society of America Bulletin 115, 1289-1306.

Table 1. List of radiocarbon data used in this study

| Calibrated Age (2σ cal yr BP) | Analytical Age (1σ 14C yr BP) | Lab Number | 13C (‰) | Site Identifier | Depth (cm) | Description of Dated Material | Type | Contact |
|---|---|---|---|---|---|---|---|---|
| | | | | **Mad River Slough** | | | | |
| 307 - 1 | 235±20 | OS-117742 | -24.84 | MR.14.02.B | 140.5-141.5cm | Herbaceous stem | Maximum | A |
| 511 - 476 | 420±15 | OS-117743 | -13.89 | MR.14.02.B | 161.5-162.5cm | Distichlis rhizome | Maximum | A |
| 956 - 802 | 990±20 | OS-117744 | -11.39 | MR.14.02.B | 225.5-226cm | 2 Distichlis rhizomes | Maximum | B |
| 956 - 912 | 1000±15 | OS-119964 | -26.65 | MR.14.05.B | 188.5-189cm | Herbaceous stem | Maximum | B |
| 1057 - 961 | 1100±20 | OS-117822 | -24.8 | MR.14.02.A | 273-273.5cm | Detrital grindelia stem | Minimum | C |
| 1280 - 1183 | 1290±15 | OS-119965 | -25.69 | MR.14.05.C | 246-247cm | Rhizome | Maximum | C |
| 1690 - 1545 | 1690±20 | OS-118743 | -25.57 | MR.14.02.A | 297.50-298.25cm | ~25 seeds (atriplex and potamogeton) | Maximum | D |
| | | | | **McDaniel Slough** | | | | |
| 283 - 1 | 170±15 | OS-119960 | -24.32 | MD.14.03.C | 117-118cm | Herbaceous stem | Maximum | A |
| 926 - 798 | 955±15 | OS-119963 | -25.64 | MD.14.06.C | 168.5-169.5cm | Rhizome | Minimum | B |
| 951 - 804 | 990±15 | OS-117738 | -26.03 | MD.14.06.C | 169.5-170.5cm | 2 rhizomes | Maximum | B |
| 965 - 929 | 1040±15 | OS-117739 | -26.82 | MD.14.03.C | 212.5-213.5cm | Rhizome | Maximum | B |
| 1399 - 1328 | 1480±15 | OS-119962 | -27.84 | MD.14.05.A | 276-277cm | Rhizome and stem fragments | Maximum | C |
| 1707 - 1575 | 1740±15 | OS-119961 | -27.06 | MD.14.05.B1 | 306.5-307.5cm | Herbaceous stem | Minimum | D |
| 1695 - 1565 | 1720±15 | OS-117740 | -28.02 | MD.14.05.B1 | 308-309cm | 2 rhizomes | Maximum | D |
| 1708 - 1614 | 1750±15 | OS-117741 | -15.26 | MD.14.04.B | 379.5-380.5cm | Distichlis rhizome | Maximum | D |
| | | | | **Jacoby Creek** | | | | |
| 289 - 1 | 195±15 | OS-117608 | -13.5 | JC.14.02.C | 81-82cm | Distichlis rhizome | Maximum | A |
| 1263 - 1082 | 1240±20 | OS-123307 | -12.82 | JC.14.02.D | 104.5cm | Herbaceous stem (detrital?) | N/A | N/A |
| 1333 - 1285 | 1390+20 | OS-124863 | -24.62 | JC.14.02.D | 103-105cm | Potamogeton seed casings (detrital?) | N/A | N/A |
| Modern | >Modern | OS-125075 | -16.36 | JC.14.02.B | 100-101cm | Herbaceous stem (detrital?) | N/A | N/A |
| 1166 - 968 | 1130±20 | OS-119878 | -26.64 | JC.14.02.D | 130-130.5cm | Rhizome | Minimum | C |
| 1277 - 1181 | 1280±20 | OS-117609 | -27.65 | JC.14.02.C | 125.5-126cm | Rhizome fragments | Maximum | C |
| 1692 - 1561 | 1710±15 | OS-119959 | -28.43 | JC.14.02.C | 167.5-168cm | Wood frament (detrital) | Minimum | D |
| 1694 - 1558 | 1710±20 | OS-117610 | -27.4 | JC.14.02.C | 170-171.5cm | Rhizome or stem | Maximum | D |

Table 2. Diatom taxa observed in surface samples from tidal flats and marshes along northern Humboldt Bay.

| Diatom species | N | Hill's N2 | Diatom species | N | Hill's N2 |
|---|---|---|---|---|---|
| *Achnanthes brevipes* | 55 | 11.999 | *Gyrosigma balticum* | 24 | 7.735 |
| *Achnanthes separata* | 16 | 11.119 | *Gyrosigma eximium* | 39 | 17.531 |
| *Aulacodiscus kittonii* | 1 | 1.000 | *Gyrosigma fasciola* | 2 | 2.000 |
| *Aulacodiscus margaritaceus* | 3 | 1.354 | *Gyrosigma spp undiff* | 10 | 7.353 |
| *Auliscus sculptus* | 2 | 2.000 | *Gyrosigma wansbeckii* | 30 | 6.351 |
| *Amphora acutiuscula* | 1 | 1.000 | *Hantzschia amphioxys* | 6 | 3.879 |
| *Amphora holsatica* | 4 | 1.963 | *Hippodonta hungarica* | 3 | 2.687 |
| *Amphora libyca* | 1 | 1.000 | *Hyaloiscus laevis* | 18 | 12.253 |
| *Bacillaria paxillifer* | 27 | 6.331 | *Hyalodiscus scoticus* | 1 | 1.000 |
| *Biremis lucens* | 1 | 1.000 | *Hyalosynedra laevigata* | 2 | 1.993 |
| *Caloneis bacillum* | 16 | 6.003 | *Ismthia nervosa* | 1 | 1.000 |
| *Caloneis westii* | 50 | 14.846 | *Luticola mutica* | 40 | 6.742 |
| *Caloneis westii var. 1* | 10 | 7.704 | *Mastogloia elliptica* | 29 | 3.432 |
| *Campylodiscus echineis* | 30 | 13.254 | *Mastogoia exiqua* | 15 | 7.518 |
| *Campylodiscus fastuoso* | 25 | 16.936 | *Melosira moniliformis* | 43 | 15.964 |
| *Cocconeis californica* | 1 | 1.000 | *Melosira nummuloides* | 43 | 17.263 |
| *Cocconeis costata* | 26 | 8.146 | *Navicula agnita* | 15 | 4.125 |
| *Cocconeis dirupta* | 2 | 1.868 | *Navicula arenaria* | 7 | 3.282 |
| *Cocconeis disculoides* | 3 | 2.937 | *Navicula atwaterii* | 7 | 6.796 |
| *Cocconeis sp HB1* | 17 | 1.647 | *Navicula cincta* | 11 | 5.837 |
| *Cocconeis sp HB2* | 32 | 7.966 | *Navicula cryptotenella* | 31 | 12.999 |
| *Cocconeis pellucida* | 1 | 1.000 | *Navicula digitoradiata* | 12 | 4.809 |
| *Cocconeis peltoides* | 24 | 5.663 | *Navicula directa* | 11 | 8.646 |
| *Cocconeis parva* | 7 | 3.292 | *Navicula eidrigiana* | 6 | 3.929 |
| *Cocconeis scutellum* | 40 | 10.018 | *Navicula flagellifera* | 3 | 2.556 |
| *Cocconeis vetusta* | 2 | 2.000 | *Navicula gregaria* | 6 | 4.118 |
| *Cosmioneis delawarensis* | 3 | 2.530 | *Navicula sp. HB1* | 17 | 4.048 |
| *Cosmioneis pusilla* | 12 | 5.058 | *Navicula kefingensis* | 3 | 2.229 |
| *Delphineis margaritalimbata* | 9 | 3.907 | *Navicula microdigitoradiata* | 17 | 2.540 |
| *Delphineis surirella* | 2 | 1.650 | *Navicula peregrina* | 27 | 11.158 |
| *Denticula subtilis* | 29 | 11.874 | *Navicula phylleptosoma* | 1 | 1.000 |
| *Diadesmis contenta* | 6 | 3.664 | *Navicula peregrinopsis* | 9 | 4.418 |
| *Diploneis bombus* | 29 | 13.037 | *Navicula salinarum* | 10 | 4.262 |
| *Diploneis decipiens var. parallela* | 27 | 10.091 | *Navicula slesvicensis* | 8 | 5.019 |
| *Diploneis didyma* | 27 | 10.322 | *Navicula vaneii* | 5 | 3.925 |
| *Diploneis elliptica* | 28 | 9.243 | *Nitzschia bilobata* | 7 | 4.238 |
| *Diploneis elliptica f. rhombica* | 25 | 7.966 | *Nitzschia brevissima* | 16 | 5.595 |
| *Diploneis gruendleri* | 8 | 5.517 | *Nitzschia fasciculata* | 30 | 7.554 |
| *Diploneis interrupta* | 19 | 7.287 | *Nitzschia improvisa cf* | 29 | 7.101 |
| *Diploneis litoralis var. clathrata* | 36 | 11.396 | *Nitzschia lorenziana* | 2 | 2.000 |
| *Diploneis pseudovalis* | 30 | 6.524 | *Nitzschia scapelliformis* | 24 | 9.443 |
| *Diploneis smithii* | 19 | 9.691 | *Nitzschia sigma* | 51 | 28.839 |
| *Diploneis smithii var. dilatata* | 7 | 1.452 | *Nitzschia aff sigmoides* | 8 | 4.239 |
| *Diploneis stroemii* | 14 | 4.949 | *Nitzschia vitrea* | 16 | 4.635 |
| *Endictya hendeyi* | 16 | 10.940 | *Odontella aurita* | 1 | 1.000 |
| *Endictya oceanica* | 11 | 7.528 | *Opephora minuta* | 1 | 1.000 |
| *Entomoneis alata* | 5 | 4.390 | *Paralia fenestrata* | 27 | 14.176 |
| *Fallacia pygmaea* | 20 | 6.285 | *Paralia sulcata* | 36 | 17.495 |
| *Fragilaria investiens* | 1 | 1.000 | *Paralia sulcata small form* | 51 | 24.232 |
| *Frustulia linkeii* | 12 | 4.915 | *Petroneis granulata* | 8 | 6.245 |
| *Frustulia vulgaris* | 2 | 1.981 | *Pinnularia borealis* | 6 | 2.528 |

Table 2 (cont). Diatom taxa observed in surface samples from tidal flats and marshes along northern Humboldt Bay.

| Diatom species | N | Hill's N2 | Diatom species | N | Hill's N2 |
|---|---|---|---|---|---|
| *Pinnularia lagerstedtii* | 10 | 6.343 | **Planktonic taxa** | | |
| *Placoneis delicatula* | 8 | 4.201 | *Actinoptychus senarius* | 18 | 12.826 |
| *Pleurosigma angulata* | 12 | 4.976 | *Actinocyclus aff giant valve* | 24 | 12.534 |
| *Parlibellus delongii* | 1 | 1.000 | *Actinocyclus spp* | 3 | 2.679 |
| *Petrodictyon gemma* | 1 | 1.000 | *Chaetoceros spp* | 11 | 5.579 |
| *Rhaphoneis amphiceros* | 8 | 7.032 | *Coscinodiscus marginatus* | 4 | 3.634 |
| *Rhaphoneis psammicola* | 16 | 6.912 | *Coscinodiscus radiatus* | 7 | 6.563 |
| *Rhopalodia acuminata* | 4 | 3.999 | *Stephanopyxis spp* | 10 | 8.794 |
| *Rhopalodia brebissonii* | 37 | 11.987 | *Thalassiosira eccentrica* | 6 | 4.915 |
| *Rhopalodia constricta* | 11 | 7.157 | *Thalassiosira spp* | 13 | 8.945 |
| *Rhopalodia musculus* | 17 | 6.890 | *Thalassionema nitzschioides* | 3 | 2.999 |
| *Rhopalodia sp HB1* | 1 | 1.000 | | | |
| *Rhoicosphenia marina* | 9 | 7.056 | | | |
| *Scolioneis tumida* | 26 | 14.549 | | | |
| *Seminavis sp 1* | 10 | 1.904 | | | |
| *Surirella brebissonii* | 11 | 9.266 | | | |
| *Surirella fastuosa* | 43 | 8.911 | | | |
| *Surirella sp HB1* | 5 | 3.793 | | | |
| *Surirella scalaris* | 9 | 7.366 | | | |
| *Tabularia fasciculata* | 41 | 8.518 | | | |
| *Trachyneis aspera* | 34 | 13.720 | | | |
| *Trachyneis aspera var. 1* | 3 | 2.263 | | | |
| *Tryblionella acuminata* | 14 | 10.128 | | | |
| *Tryblionella apiculata* | 46 | 25.546 | | | |
| *Tryblionella* sp 1 | 8 | 6.593 | | | |
| *Tryblionella compressa* | 40 | 23.687 | | | |
| *Tryblionella coarctata* | 31 | 17.496 | | | |
| *Tryblionella debilis* | 28 | 3.982 | | | |
| *Tryblionella granulata* | 53 | 19.166 | | | |
| *Tryblionella hungarica cf* | 1 | 1.000 | | | |
| *Tryblionella levidensis* | 9 | 5.979 | | | |
| *Tryblionella littoralis* | 3 | 2.999 | | | |
| *Tryblionella navicularis* | 39 | 15.993 | | | |
| *Tryblionella pararostata* | 7 | 4.058 | | | |
| *Tryblionella parasitica* | 28 | 18.852 | | | |
| *Tryblionella rorida* | 16 | 8.788 | | | |
| *Tryblionella subconstricta* | 3 | 2.995 | | | |
| *Tryblionella vexans* | 7 | 4.228 | | | |

Table 3. List of diatom taxa indicated by numbers in Figure 8.

| | | | |
|---|---|---|---|
| 1 | *Hantzschia amphioxys* | 30 | *Tryblionella apiculata* |
| 2 | *Pinnularia lagerstedtii* | 31 | *Navicula digitoradiata* |
| 3 | *Luticola mutica* | 32 | *Tryblionella navicularis* |
| 4 | *Nitzschia brevissima* | 33 | *Caloneis westii* |
| 5 | *Cosmioneis pusilla* | 34 | *Tryblionella levidensis* |
| 6 | *Frustulia linkeii* | 35 | *Diploneis decipiens* var. *paralella* |
| 7 | *Navicula salinarum* | 36 | *Trachyneis aspera* |
| 8 | *Navicula peregrina* | 37 | *Cocconeis scutellum* |
| 9 | *Fallacia pygmaea* | 38 | *Surirella fastuosa* |
| 10 | *Tryblionella debilis* | 39 | *Cocconeis costata* |
| 11 | *Caloneis bacillum* | 40 | *Tryblionella rorida* |
| 12 | *Diploneis interrupta* | 41 | *Tryblionella pararostata* |
| 13 | *Denticula subtilis* | 42 | *Nitzschia fasciculata* |
| 14 | *Diploneis pseudovalis* | 43 | *Gyrosigma balticum* |
| 15 | *Navicula cincta* | 44 | *Cocconeis parva* |
| 16 | *Diploneis stroemii* | 45 | *Seminavis* sp 1 |
| 17 | *Tryblionella vexans* | 46 | *Tryblionella coarctata* |
| 18 | *Gyrosigma eximium* | 47 | *Petroneis granulata* |
| 19 | *Diploneis smithii* | 48 | *Scolioneis tumida* |
| 20 | *Nitzschia sigma* | 49 | *Endictya hendeyi* |
| 21 | *Rhopalodia brebissonii* | 50 | *Rhaphoneis psammicola* |
| 22 | *Melosira nummuloides* | 51 | *Melosira moniliformis* |
| 23 | *Nitzschia vitrea* | 52 | *Tryblionella acuminata* |
| 24 | *Nitzschia scapelliformis* | 53 | *Cocconeis sp HB2* |
| 25 | *Rhopalodia musculus* | 54 | *Paralia fenestrata* |
| 26 | *Mastogloia elliptica* | 55 | *Delphineis margaritalimbata* |
| 27 | *Achnanthes brevipes* | 56 | *Diploneis bombus* |
| 28 | *Nitzschia improvisa cf* | 57 | *Rhoicosphenia marina* |
| 29 | *Gyrosigma wansbeckii* | 58 | *Tabularia fasciculata* |

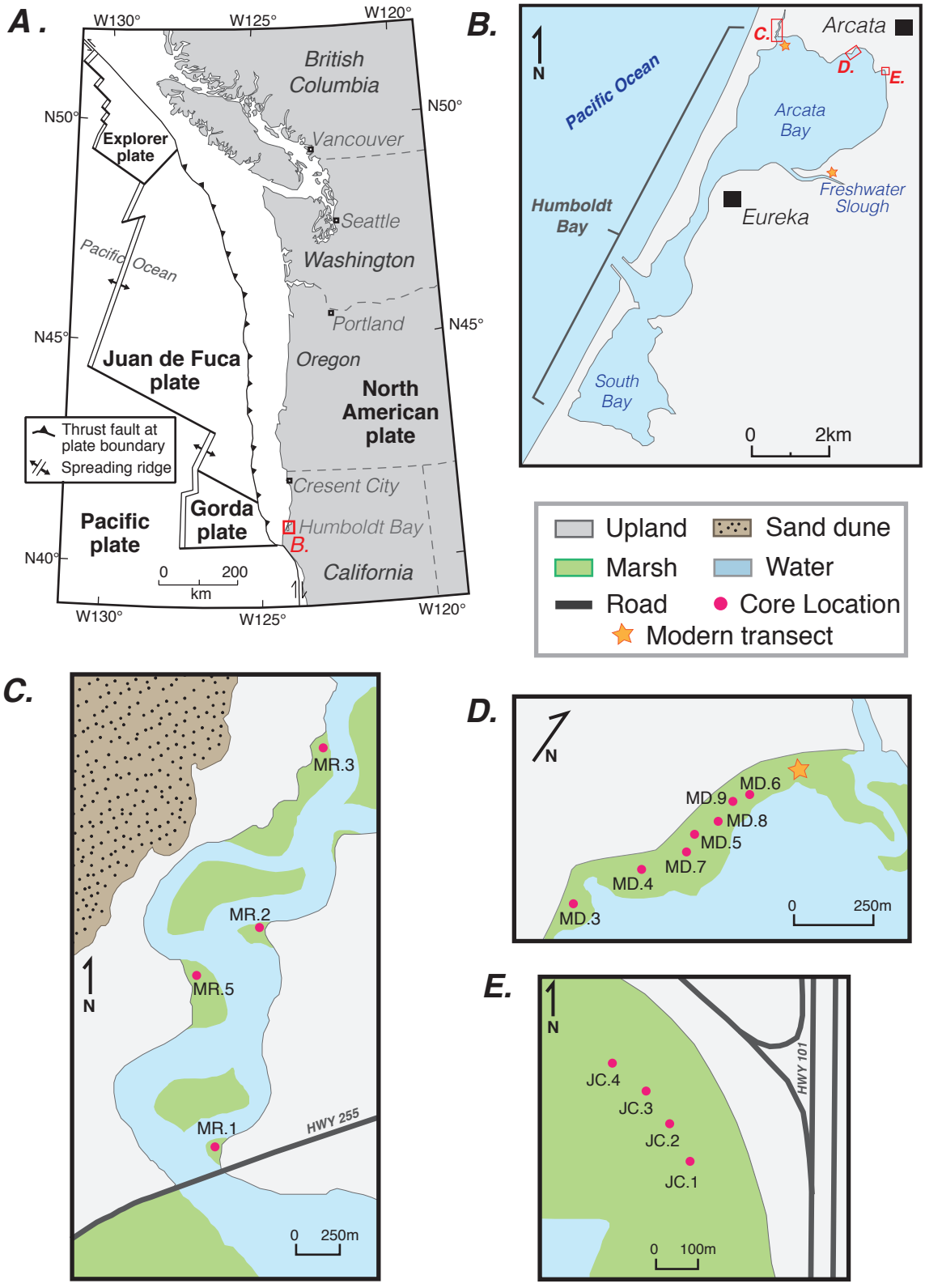


Figure 1. A) Lambert conformal projection of Cascadia coastal margin. B) Map showing Arcata Bay, the northern lobe of Humboldt Bay, California. C) Map showing core locations at Mad River Slough. D) Map showing core locations at MacDaniel Slough. E) Map showing core locations at Jacoby Creek.

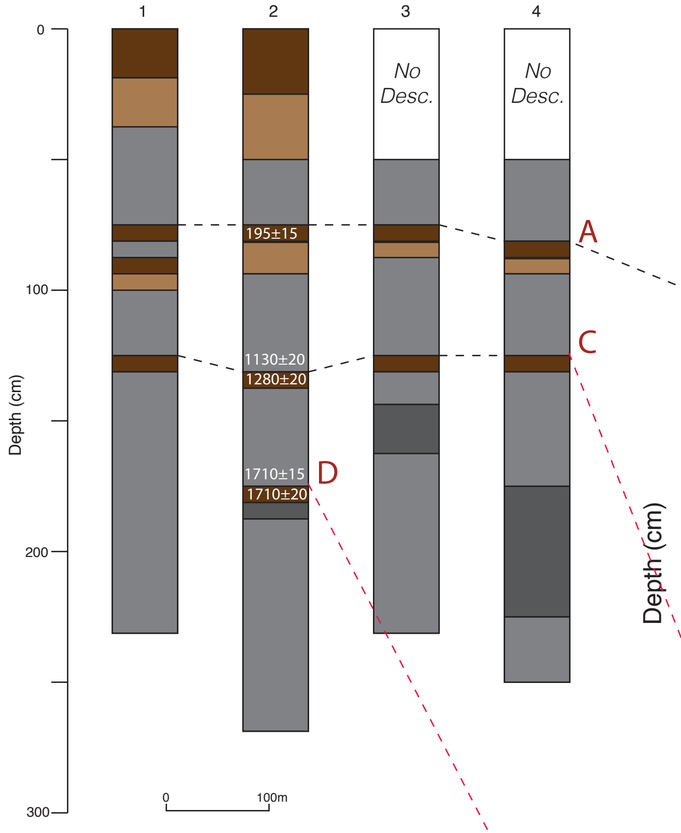


Figure 2a. Stratigraphy of the Jacoby Creek salt marsh location with radiocarbon ages (white numbers) and regional correlations (red dashed lines).

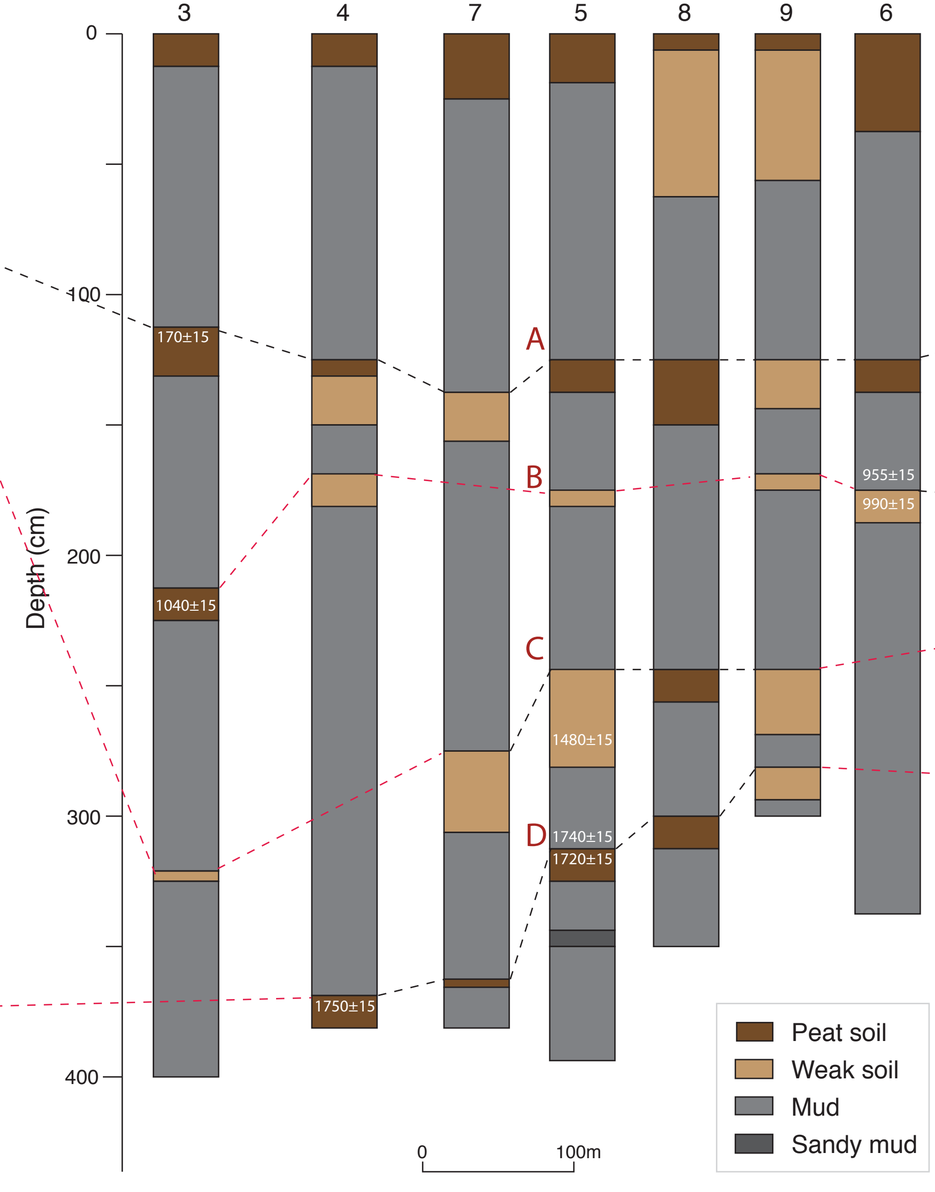


Figure 2b. Stratigraphy of the McDaniel Slough salt marsh location with radiocarbon ages (white numbers) and regional correlations (red dashed lines).

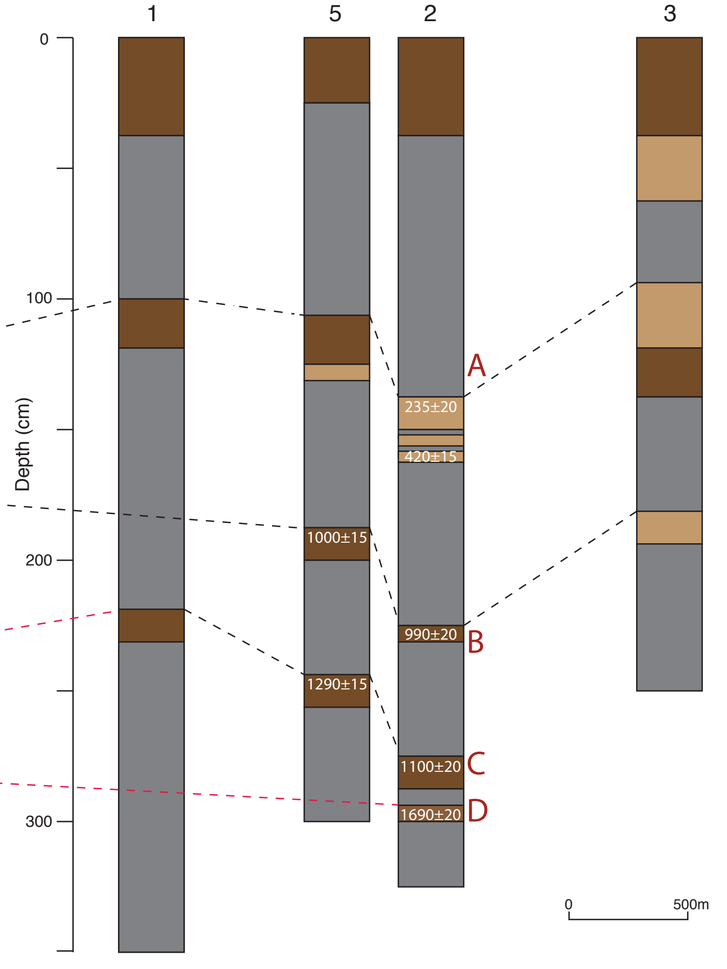


Figure 2c. Stratigraphy of the Mad River Slough salt marsh location with radiocarbon ages (white numbers) and regional correlations (red dashed lines).

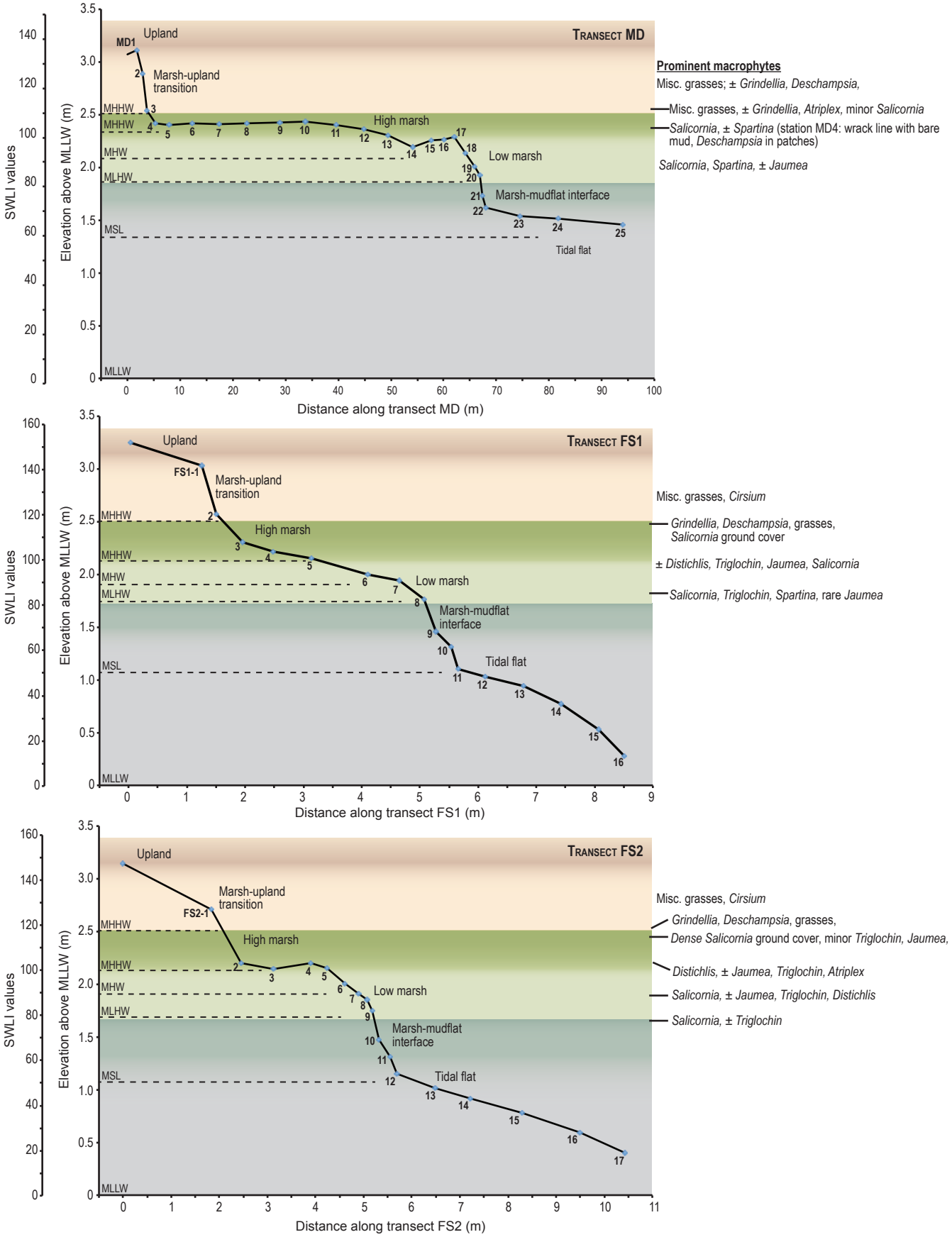


Figure 3. Profiles of sampling transects along northern Humboldt Bay to document modern distributions of benthic diatoms. (A) Transect "MD" from a marsh adjacent to McDaniel Slough; (B and C) transects "FS1" and "FS2" from fringing salt marshes at Fay Slough. Prominent vascular plant taxa at different elevations for each location are listed to the right of each diagram. SWLI = Standardized Water Level Index

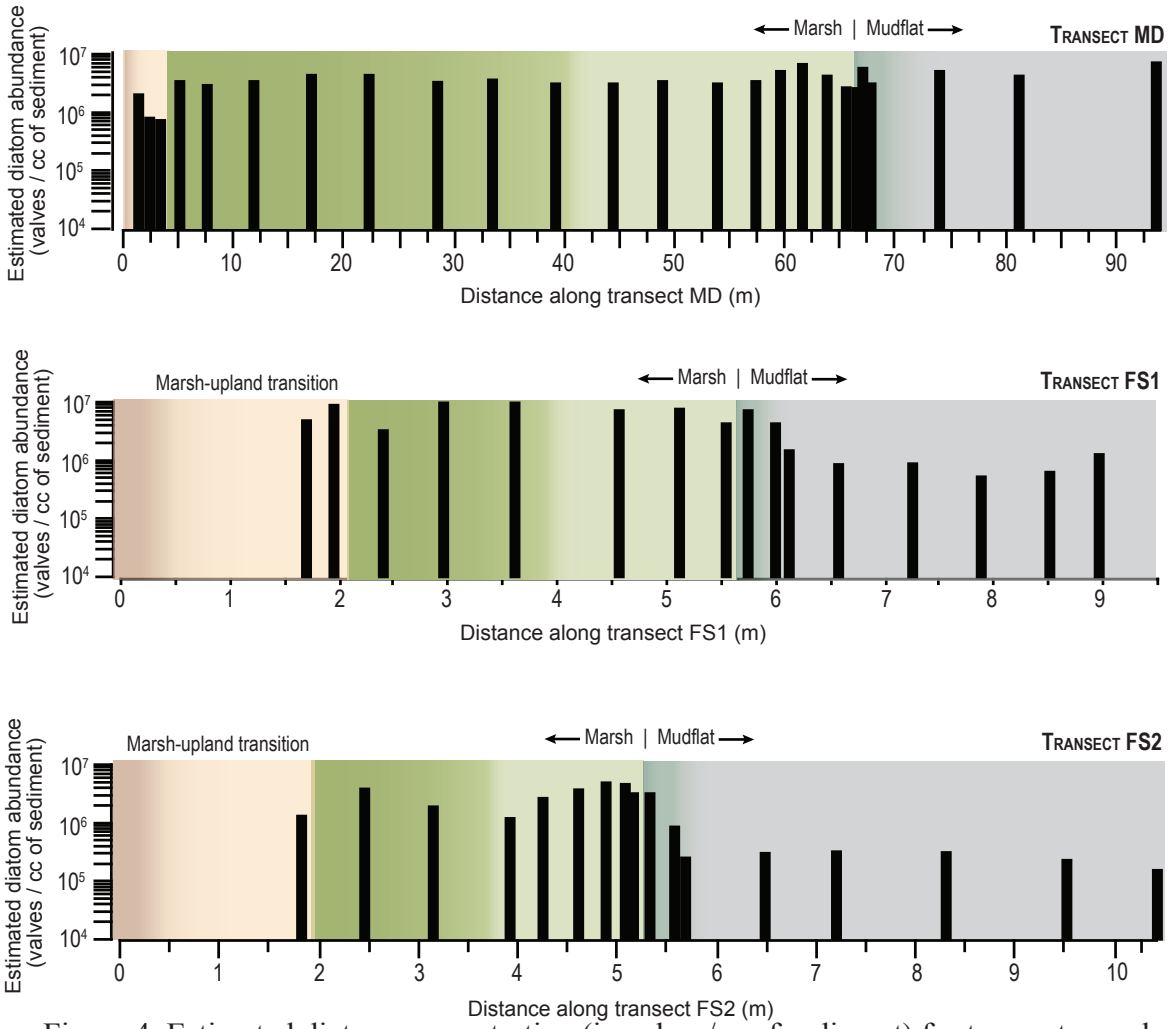


Figure 4. Estimated diatom concentration (in valves/cc of sediment) for transect samples.

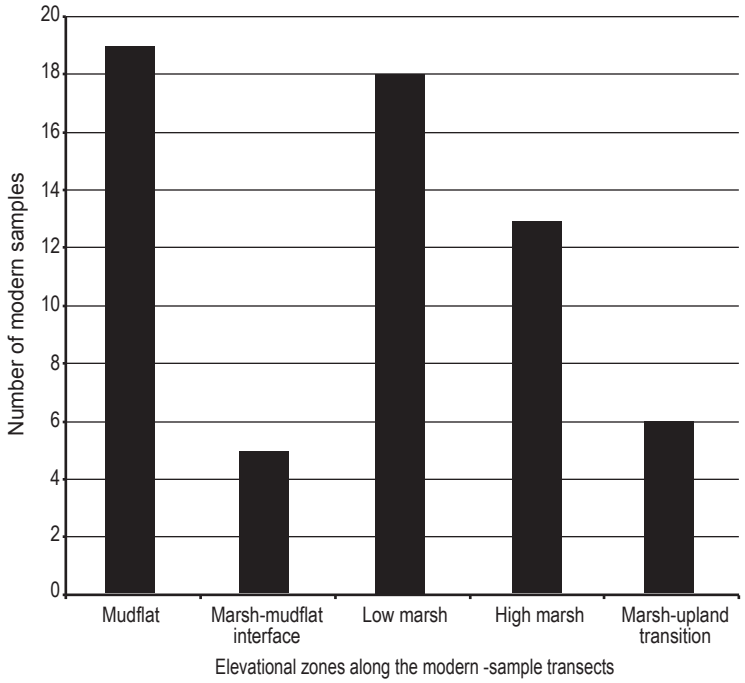


Figure 5. Numbers of modern samples collected from different elevational zones.

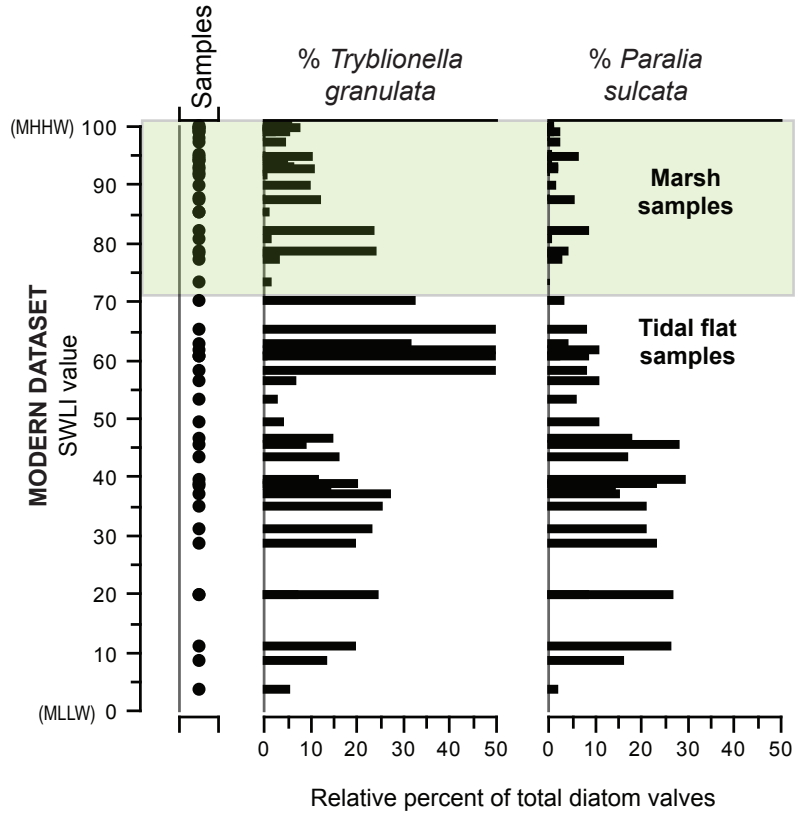


Figure 6. Distributions and relative abundances of *Paralia sulcata* and *Tryblionella granulata* in modern mudflat and marsh samples from Humboldt Bay. SWLI = Standardized Water Level Index

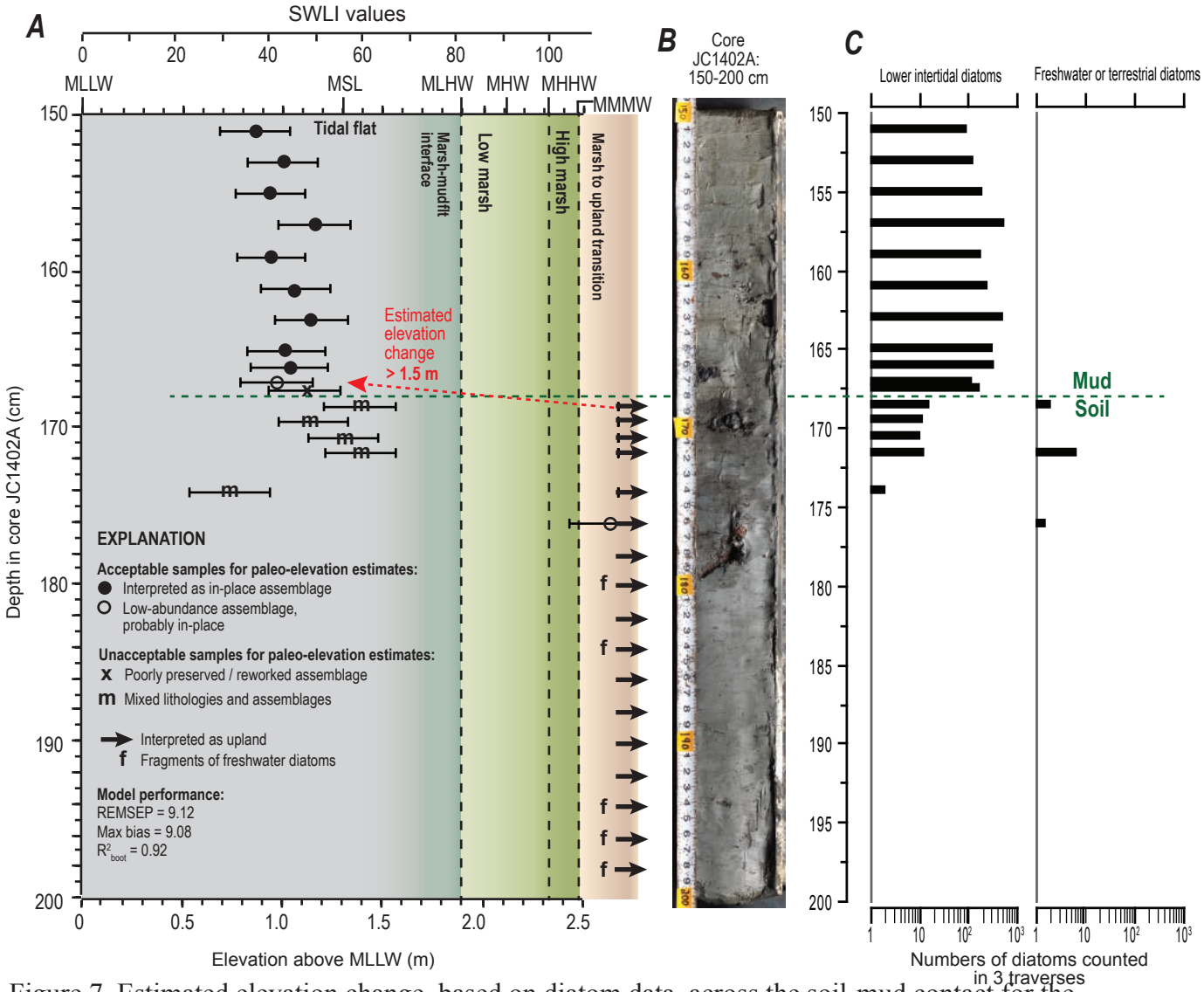


Figure 7. Estimated elevation change, based on diatom data, across the soil-mud contact for the 1634-1560 cal yr BP event at Jacoby Creek. (A) Transfer-function estimate of > 1.5 m based on an interpretation of a shift from an upland environment to a mudflat environment. The soil is basically devoid of diatom except for a few freshwater species and tidal flat taxa mixed in from overlying mud. Marsh taxa are not observed in either the soil or overlying mud. (B) Photomosaic of core JC1402A: 150-200 cm. (C) Comparison of diatom abundance between the soil and overlying mud. Note the log scale. Deposits below 175 cm contain rare fragments of freshwater diatoms and phytoliths, consistent with an upland deposit. SWLI = Standardized Water Level Index

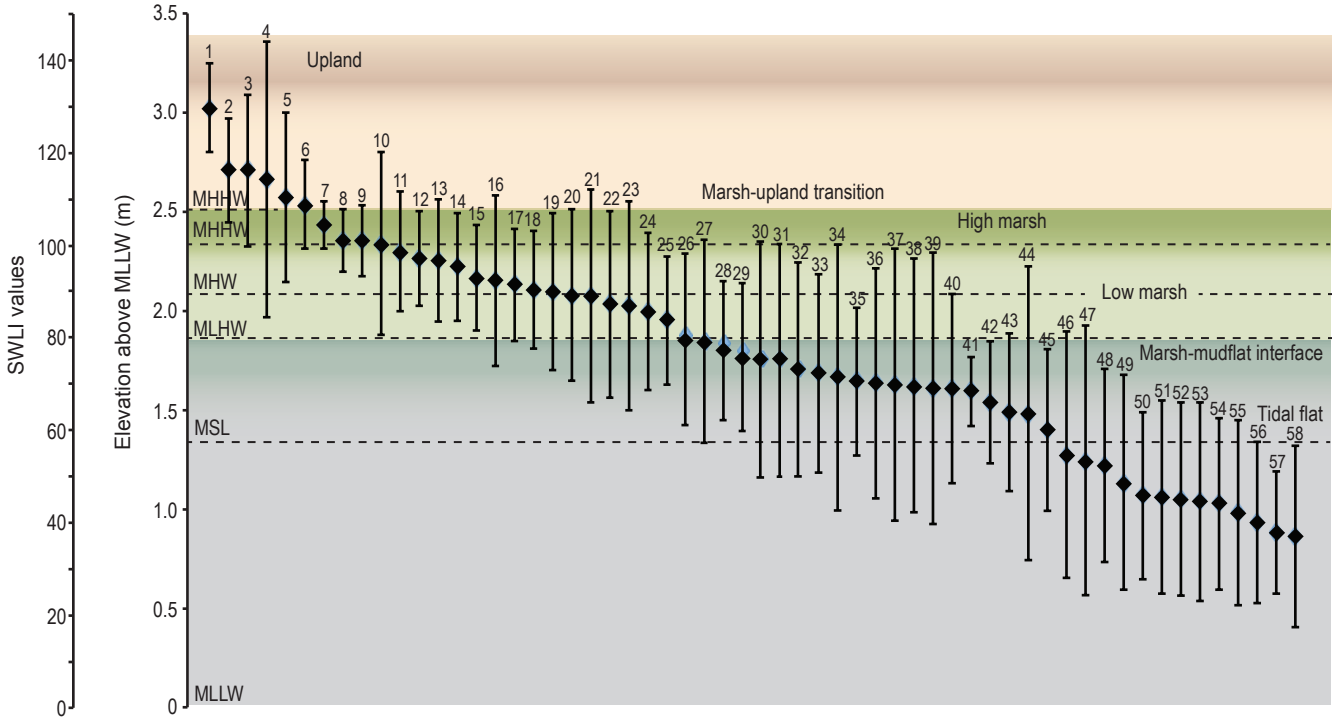


Figure 8. Modern elevation ranges, based on data from 61 modern intertidal transect samples, of some of the more common diatoms observed in samples from Jacoby Creek cores. The dominant or "optimum" elevation is shown by a black diamond; vertical lines indicate the estimated distributional range, or "tolerance." Numbers above the data points refer to species listed in Table 3. SWLI = Standardized Water Level Index

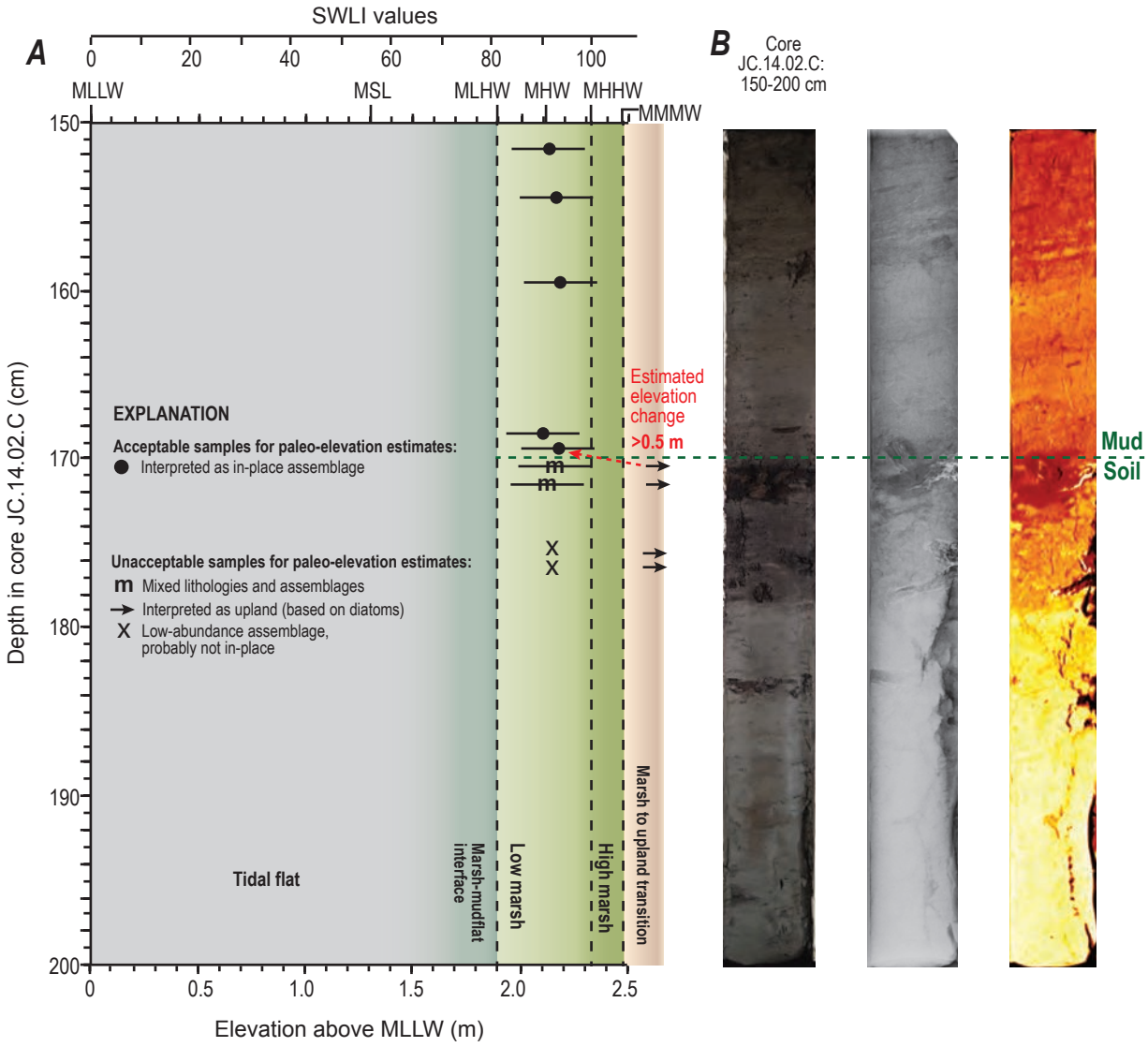


Figure 9. Estimated elevation change, based on foraminiferal data, across the soil-mud contact for the 1634-1560 cal yr BP event at Jacoby Creek. (A) Transfer-function estimate of > 0.5 m based on an interpretation of a shift from the same upland environment identifed by the diatom analysis to a low to middle marsh environment. (B) Photomosaic, x-ray and CT of core JC1402C: 150-200 cm. SWLI = Standardized Water Level Index

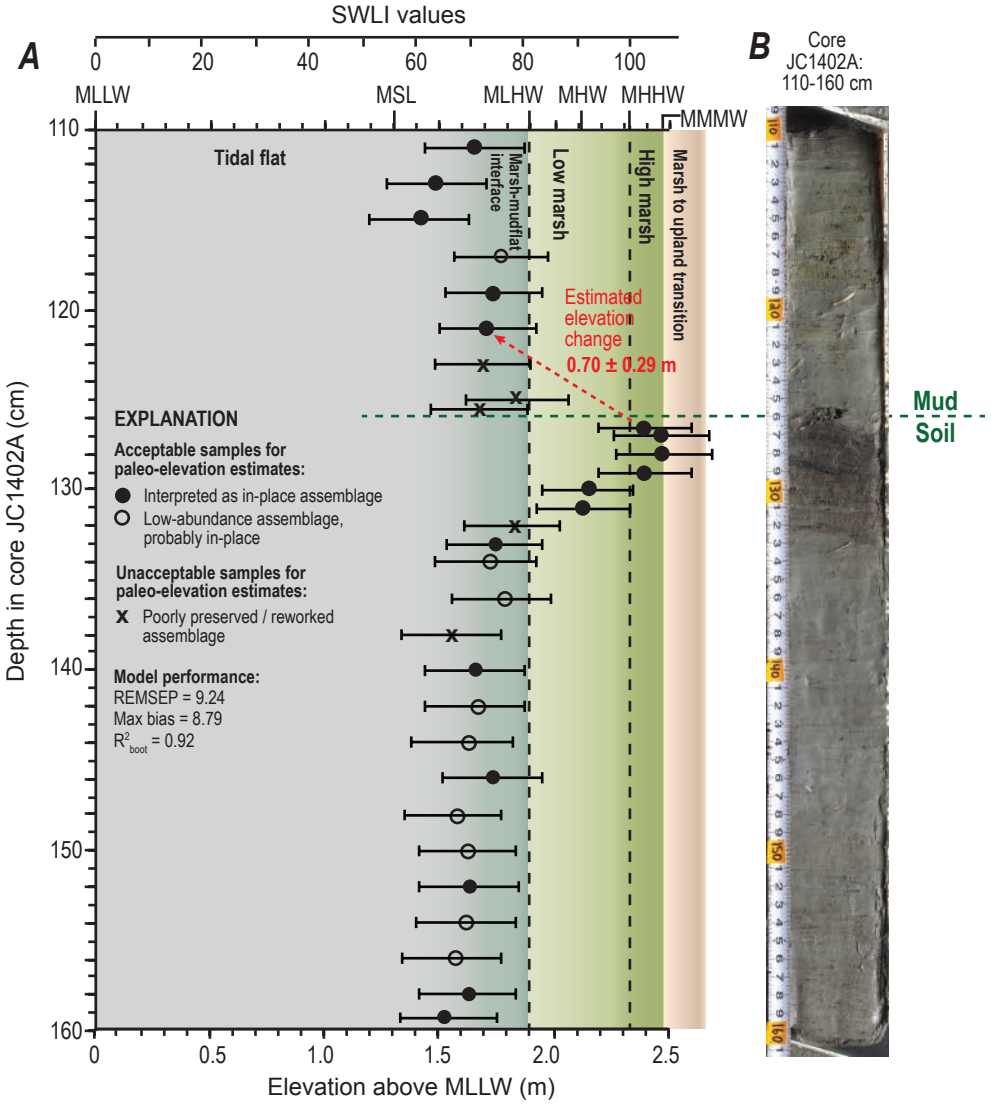


Figure 10. Estimated elevation change, based on diatom data, across the soil-mud contact for the 1235-1018 cal yr BP event at Jacoby Creek. (A) Transfer-function estimate of 0.70 ± .29 m based on an interpretation of a shift from a dry high marsh soil, with common aerophilous diatoms, to a mudflat environment. The first sample above the soil-mud contact that is interpreted to be in place is at 122 cm; the intervening samples from mud directly above the soil contain a mix of poorly preserved taxa indicating a reworked deposit. (B) Photomosaic of core JC1402A: 110-160 cm. SWLI = Standardized Water Level Index

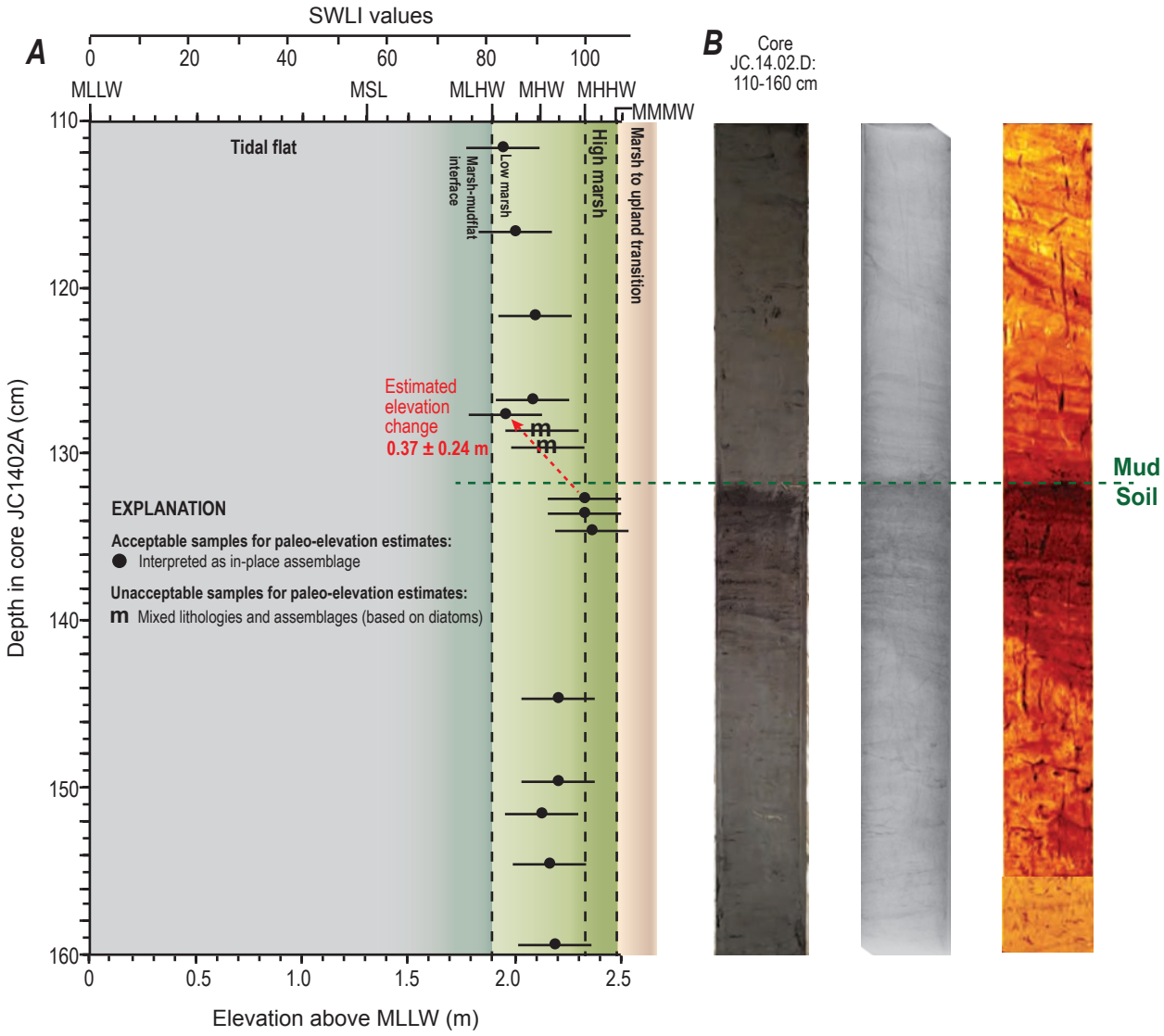


Figure 11. Estimated elevation change, based on foraminiferal data, across the soil-mud contact for the 1235-1018 cal yr BP event at Jacoby Creek. (A) Transfer-function estimate of 0.37 ± 0.24 m based on an interpretation of a shift from a high marsh environment to a low to middle marsh environment. (B) Photo-mosaic, x-ray and CT of core JC1402D: 110-160 cm. SWLI = Standardized Water Level Index

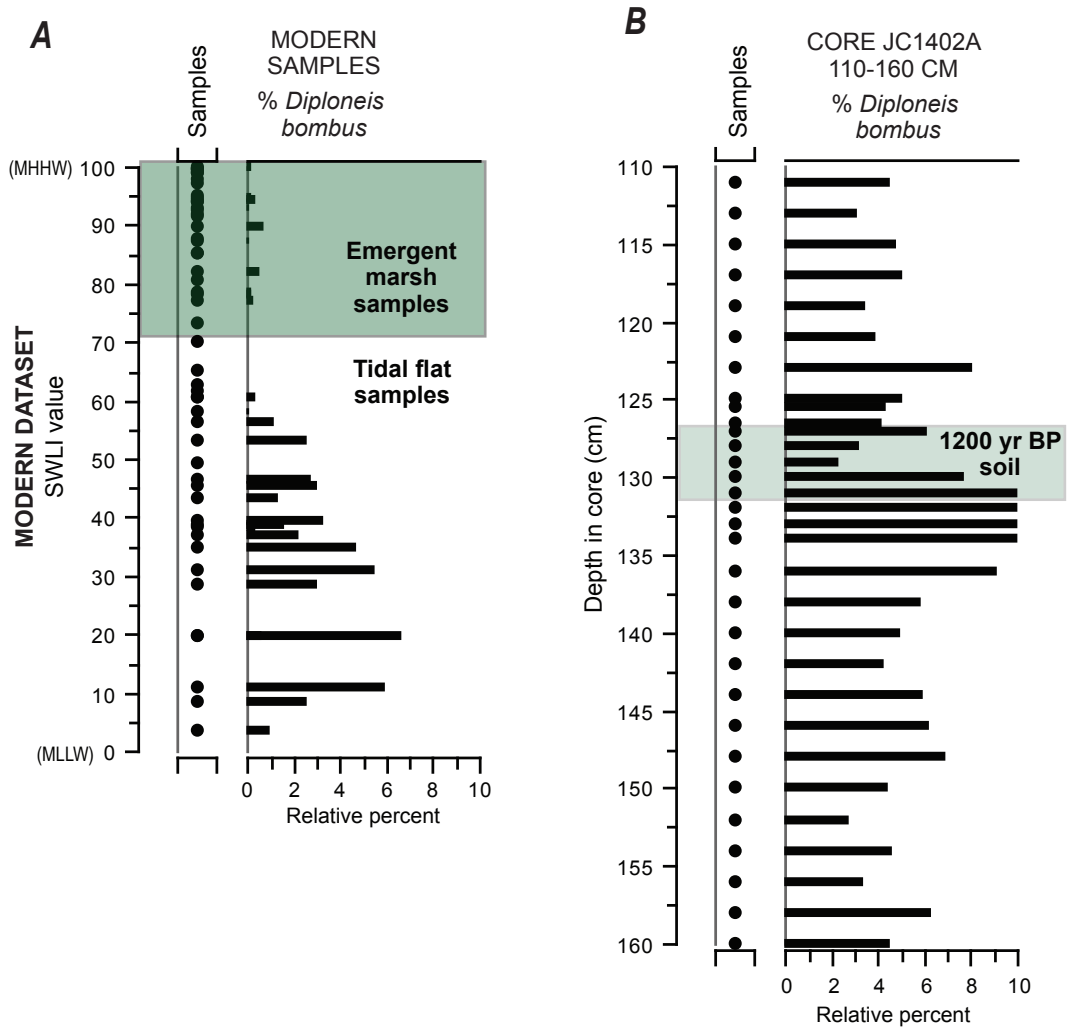


Figure 12. Comparisons of relative abundance of *Diploneis bombus* in (A) modern-transect samples; and (B) samples from core JC1402A: 110-160 cm, which includes the 1235-1018 cal yr BP soil. SWLI = Standardized Water Level Index

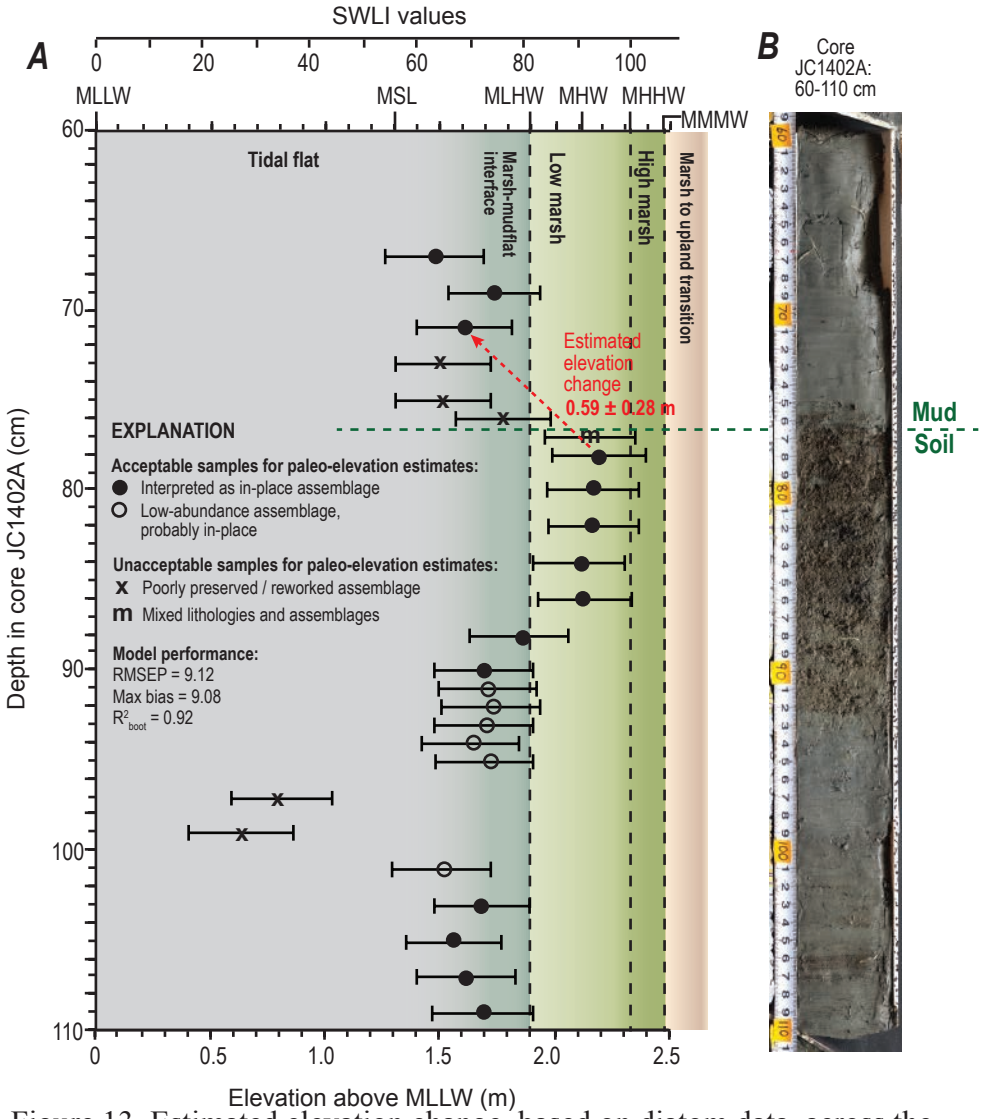


Figure 13. Estimated elevation change, based on diatom data, across the soil-mud contact for the 250 yr BP (AD 1700) event at Jacoby Creek. (A) Transfer-function estimate of 0.59 ± .28 m is based on an interpretation of a shift from a regularly flooded high marsh to a mudflat. The first sample above the soil-mud contact that is interpreted to be in place is at 73 cm; poorly preserved taxa in the intervening samples indicate a reworked deposit. The sample from just below the disrupted soil-mud contact at 77 cm is interpreted as containing a mix of taxa from the peat and overlying mud, and therefore not representative of the paleo-soil environment. (B) Photomosaic of core JC1402A: 110-160 cm. SWLI = Standardized Water Level Index

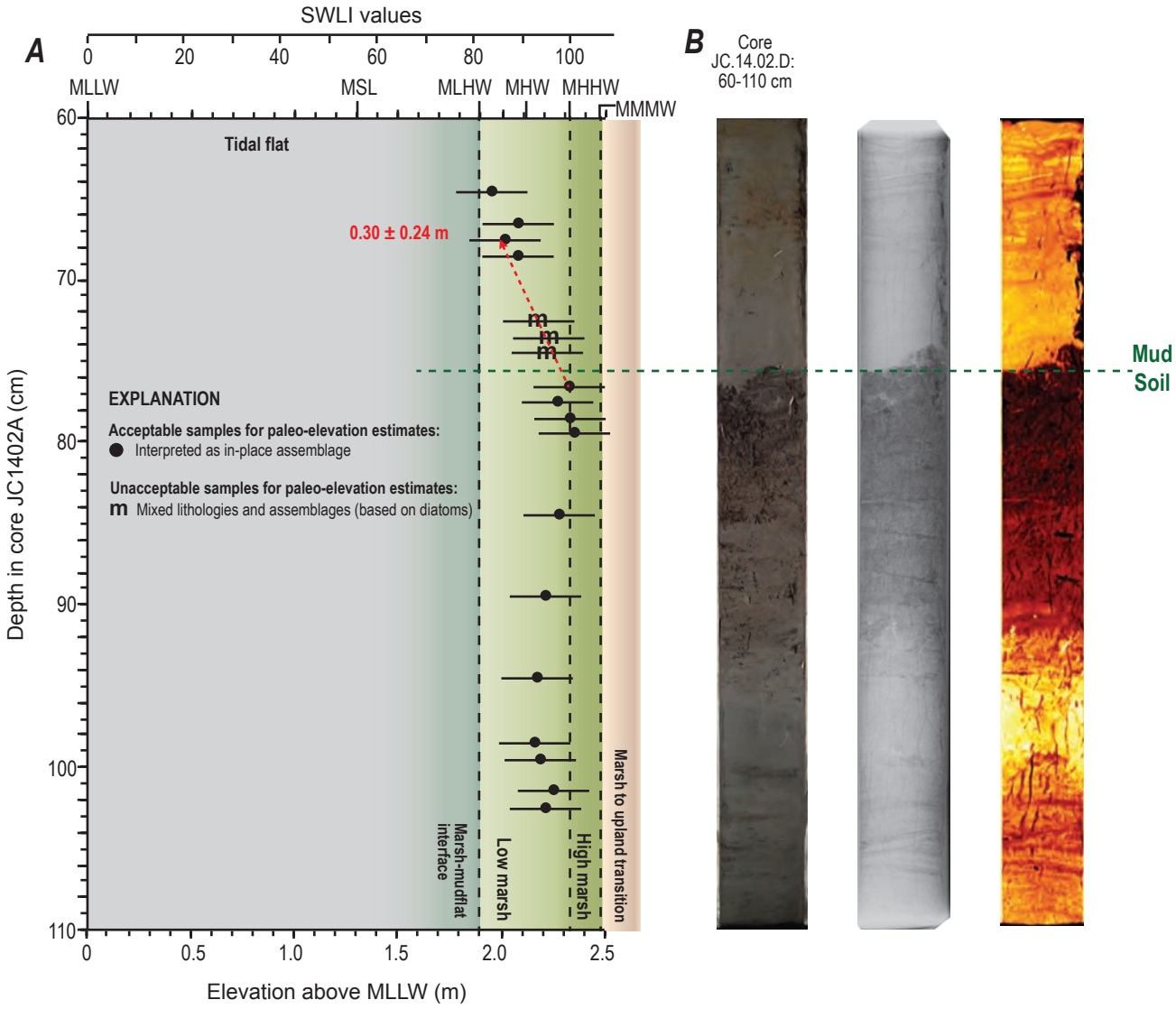


Figure 14. Estimated elevation change, based on foraminiferal data, across the soil-mud contact for the 250 yr BP event at Jacoby Creek. (A) Transfer-function estimate of 0.30 ± 0.24 m based on an interpretation of a shift from a high marsh environment to a low to middle marsh environment. (B) Photomosaic, x-ray and CT of core JC1402D: 60-110 cm. SWLI = Standardized Water Level Index